AN ABSTRACT OF THE THESIS OF

Michael Stringham for the degree of Master of Science in Nuclear Engineering

presented on June 24, 2003.

Title: Predicting Dose and Cell Survival Distributions for Brachytherapy Sources.

Redacted for privacy

Abstract approved: _____

Todd S. Palmer

The focus of this thesis is to determine the biological impact of dose from brachytherapy sources commonly used in cancer treatment. To achieve this goal, the Monte Carlo code PENELOPE was used to simulate point sources of four different isotopes (^{103}Pd, ^{125}I, ^{137}Cs, and ^{90}Sr) in an infinite medium of water. These dose distributions were then post processed, using the linear quadratic equation, to calculate cell survivability distributions and to produce 3D maps of arrays of identical sources.

Parametric studies performed with a simple shielding model showed several important trends in the data: as particle emission intensity increases killing radius (defined as the radius from the source at which only 10^{-9} of the cells will survive) increases, as the shielding attenuation factor increases kill radius decreases, as the

linear lesion coefficient (α) increases the kill radius increases, as the quadratic lesion coefficient (β) increases the kill radius increases weakly, as the isotopic decay constant increases the kill radius decreases, and as the rate of DNA damage repair increases the kill radius decreases weakly.

Monte Carlo simulations of isotropic point sources showed that the difference between the kill radius and survival radius (defined as the distance from the source at which 10^{-7} of the cells survive) was smaller relative to the survival radius, for electron emitting isotopes than for photon emitting isotopes. This has been attributed to the fact that uncharged photons interact with matter through collisions, whereas, charged electrons interact through matter through collisions and Coulomb interactions. Coulomb interactions cause a continuous slowing down of the electrons, decreasing their range.

Predicting Dose and Cell Survival Distributions for Brachytherapy Sources

by

Michael J. Stringham

A THESIS

submitted to

Oregon State University

in partial fulfillment of

the requirements for the

degree of

Master of Science

Presented June 24, 2003

Commencement June 2004

Master of Science thesis of Michael J. Stringham, presented on June 24, 2003.

APPROVED:

Redacted for privacy

Major Professor, representing Nuclear Engineering

Redacted for privacy

Head of Department of Nuclear Engineering

Redacted for privacy

Dean of the Graduate School

I understand that my thesis will become part of the permanent collection of Oregon State University libraries. My signature below authorizes release of my thesis to any reader upon request.

Redacted for privacy

Michael J. Stringham, Author

ACKNOWLEDGEMENTS

First I would like to acknowledge my minor professor Dr. Jovanovic for the extra curricular projects, he championed and allowed me to be part of in my undergraduate years. Without his help getting me interested in these projects such as the NASA reduced gravity flight opportunities, I would not have even considered attending graduate school.

Next I would like to acknowledge my major professor Dr. Palmer for just about everything. From the constant difficulties learning UNIX to taking the time out of his busy schedule to help me with editing my thesis. Without his constant help I would not have been able to graduate on time.

Next I would like to acknowledge Dr. Stewart who I have to credit with helping me select my thesis topic. He has also been instrumental in helping me learn about brachytherapy in a very short time period and he has also done the majority of the coding on the program used in this thesis.

Finally I would like to acknowledge Jordan Strawn for his help in programming and methodology in calculating voxel tallies.

TABLE OF CONTENTS

TABLE OF CONTENTS (CONTINUED)

LIST OF FIGURES

LIST OF FIGURES (CONTINUED)

LIST OF TABLES

LIST OF APPENDICES

NOMENCLATURE

Symbol	Description	Units
A_0	Initial Activity of Source	[Bq]
$\dot{D}_0$	Initial Dose Rate	[Gy/hr]
$\dot{D}$ or $\dot{D}(t)$	Dose Rate at Time t	[Gy/hr]
D_T	Dose per Track	[Gy/Bq]
G	Dose Protraction Factor	[/]
k	Isotope Decay Constant	[hr^{-1}]
m	Mass of Tally Region	[kg]
N_S	Number of Sources	[/]
R	Radius from Point Source	[cm]
S	Cell Survival Probability	[/]
t	Time	[hr]
X	Source Intensity	[Gy*cm^2/hr]
α	Linear Lesion Coefficient	[Gy^{-1}]
β	Quadratic Lesion Coefficient	[Gy^{-2}]
ε	Energy Imparted	[J]
λ	Rate of DNA damage repair	[hr^{-1}]
μ	Attenuation Coefficient	[cm^{-1}]

Predicting Dose and Cell Survival Distributions for Brachytherapy Sources

1. Introduction

1.1. Introduction

The American Cancer Society predicts that in the year 2003 alone 1.3 million new cases of cancer will occur in the United States (ACS 2003). There is ongoing medical research dedicated to the detailed understanding of how cancer spreads, methods of prevention, treatment techniques, and finding a cure. Cancer is defined as a mass of aberrant cells that tend to grow in an uncontrolled fashion. Instead of dividing at a rate to support regeneration of damaged tissue, cancer cells tend to divide more frequently, such that they grow into large lumps (tumors) displacing healthy tissue. Another characteristic of cancer cells is that they can break away from the surrounding tissue matrix and spread to other parts of the body (i.e. metastasize). Cancer cells can develop in any part of the body, which leads to a great diversity of cancer types and tumors that have drastically differing properties. Difficulties inherent in cancer treatment are: the diversity in location, the differing base tissue type that the tumors develop from, and the proximity of organs critical to survival (lungs, heart, spinal cord, etc.) to the tumor site. In this thesis, we will focus on a

specific treatment modality for prostate cancer: brachytherapy. The American Cancer Society estimates that approximately 30 out of 100,000 men will die from prostate cancer (ACS 2003). In 2003 it is estimated that there will be 220,900 new cases of prostate cancer and 28,900 will die as a result (ACS 2003). Because of this even a 1% improvement in effective treatment could save hundreds of lives.

1.2. Brachytherapy

Brachytherapy is a method of treating cancerous tumors with radiation. In brachytherapy very small 'seeds' of radioactive material are implanted inside the body in the vicinity of the tumor. The seeds are either implanted permanently in the body or implanted and then removed sometime later (Veninga 2001), and their purpose is to destroy the tumor over the lifetime of the radionuclide seed.

Figure 1-1. Brachytherapy Seed.

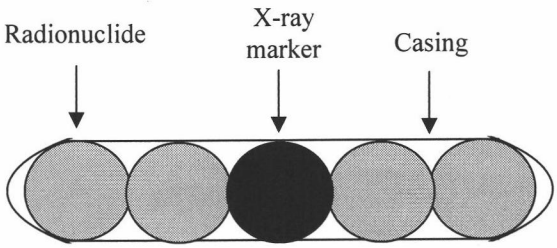

As illustrated in Figure 1-1, brachytherapy seeds are typically about 3 mm in length and 0.5 mm in diameter (AAPM 1995), and are composed of three main parts:

the radionuclide, an x-ray marker, and the casing. The radionuclide is the source of the radiation and its properties directly impact the destruction of the tumor tissue. The important properties of the radionuclide are half-life and the type and energy spectrum of the emitted radiation. The half-life is an inherent property of the radioactive material that determines how quickly it decays. It is defined as the time elapsed for half of the radionuclide (on average) to decay. Radionuclides with short half-lives will decay very quickly emitting intense radiation for a short amount of time; whereas, radionuclides with long half-lives will emit much lower intensity radiation, but over much longer times. The type of particle emitted from the radionuclide is important because differing decay types have vastly different properties. Beta radiation is the emission of a high-energy electron. Electrons are charged particles and interact with the surrounding material over a relatively short range through Coulomb interactions. Gamma radiation is the emission of high-energy photons from the radionuclide. Photons are uncharged and require collisions to slow down and deposit energy in the media that they pass through. Gamma radiation has a relatively long range. The emission spectrum is also an important factor to take into account when selecting a radionuclide for use in brachytherapy. Higher energy radiation tends to have a longer range. For example, a beta emitter that has an emission energy of 20 keV will have a range on the order of micrometers; whereas, a beta emitter that has an emission energy of about 100 keV will have a range on the order of centimeters.

An x-ray marker is placed in the brachytherapy seed to allow the treating physician to use an x-ray machine to verify that the seeds have been properly placed within the patient.

The casing of the seed is composed of a material such as titanium or stainless steel (AAPM 1995). The casing must be biologically acceptable or the body's immune system will attack it and the patient can potentially have an adverse reaction. Another major feature of the casing is that it shields the surrounding tissue from some of the radiation emitted from the source. This partial shielding can have a drastic effect upon the distribution of the energy deposited in the surrounding tissue.

The seeds are implanted in a specific pattern depending upon the location and size of the tumor and the surrounding tissue environment. Radiation is an indiscriminate killer. It will destroy any tissue within its range, whether tumor cells or healthy tissue. It is extremely important to structure the pattern of seed placement to maximize the killing to cancerous tumors while at the same time minimizing the damage to surrounding tissue and critical organs.

The placement of brachytherapy seeds has been the focus of many recent studies. For example, it is desired to have an effective kill (destruction of the tumor such that it won't grow back) by placing enough of the radionuclide into the patient such that it doesn't all decay away before it destroys all of the tumor cells (Wang

2003). The treatment plan must also avoid using excessive doses of radiation that will unnecessarily damage surrounding tissues. Another consideration is that the spacing of the seeds needs to be carefully determined such that the number of 'cold' spots within the tumor is minimized (Wu 2002), since these cold spots are the places where the radionuclide has the least chance of destroying the target cells. Again, this causes a tradeoff: more seeds makes cold spots less common, and makes shaping the radiation field easier, but more seeds is more work for the surgeon and more intrusive for the patient. The primary method for determining the distribution of radiation dose in the region to be treated with brachytherapy is by radiation transport numerical simulation.

1.3. Monte Carlo

One technique for simulating radiation transport in brachytherapy is the Monte Carlo method. Monte Carlo methods use random numbers to sample from various probability distributions to determine what will happen in a real physical situation. For the case of radiation transport, this is done by simulating the random walk traversed by a particle emitted by radioactive decay. Thousands or millions of tracks are simulated and the results are averaged to show the effect of the radiation on the region of interest.

A typical track (see Figure 1-2), begins when a random number is sampled to select a position within the radioactive source. The energy of the particle is then determined by sampling randomly from the energy spectrum of the source. Next the direction of the particle is selected with another random number. The particle moves in the selected direction and the distance to collision is calculated by sampling from a known distribution, which depends on the material properties and particle energy. Once this particle reaches its destination, an energy deposition event is sampled. If this event occurs within a region of interest, then the energy deposition is 'tallied'. The particle's energy is reduced by this amount, and a new direction is randomly sampled and the particle continues its travels. This process continues until the particle's energy drops below a user defined *cutoff energy* - the energy at which the remaining energy of the particle is deposited at the point of interaction. Many particle tracks are needed to reduce the variance in calculated statistical quantities. Radiation transport simulations predict the energy deposited in the tissue around the source, but this is only half of the problem. Biological effects must also be taken into account to determine the actual effect of the radiation upon the tumor and surrounding healthy tissue.

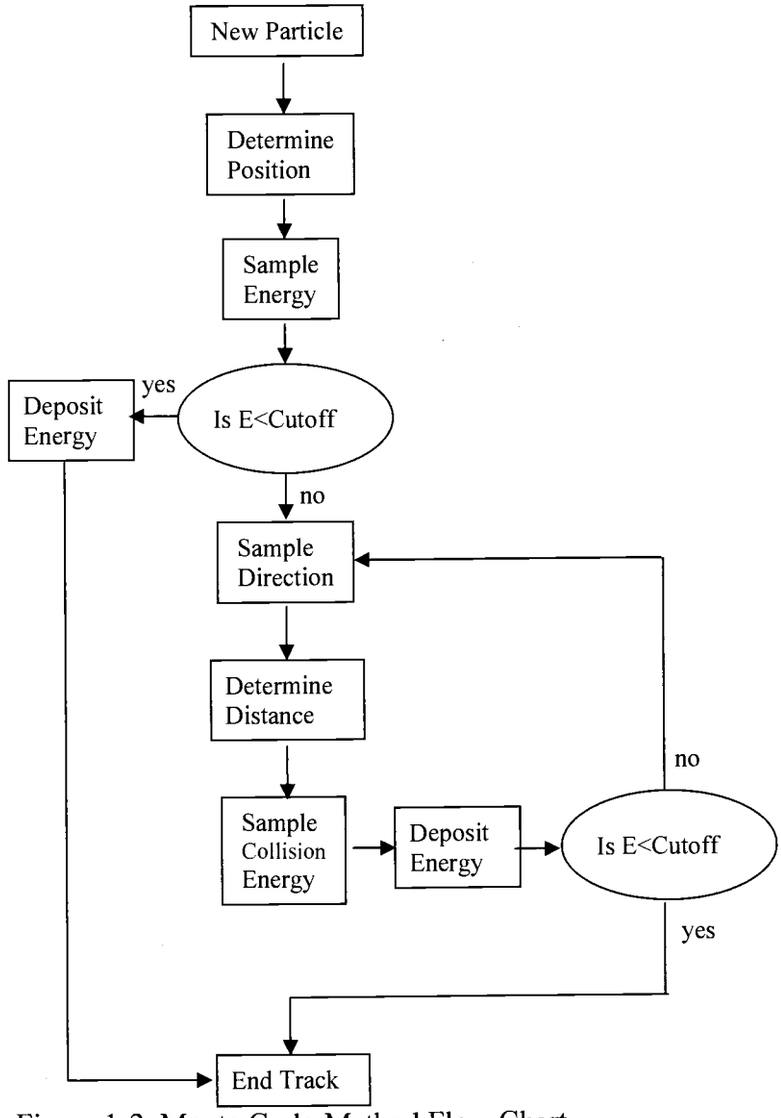

Figure 1-2. Monte Carlo Method Flow Chart.

1.4. Biological Effects

Biological mechanisms complicate the correlation between dose and cell survival. One of these mechanisms is that of DNA repair/misrepair (Sachs 1997).

When radiation is emitted from a radionuclide, a high-energy electron or photon is released which, after colliding with a chromosome within a cell, can cause a DNA strand break. This break does not necessarily mean the death of the cell because all living things have several biological methods to 'heal' themselves. The damaged DNA is detected within the cell and the cell then initiates a repair process. An interesting case occurs when a *double strand break* occurs. When two DNA strand breaks happen within 10 to 15 base pairs within a short amount of time, the situation is more complicated. These breaks when they happen close enough together can interact. When this happens, there are a variety of possible repair outcomes: a successful repair, a fatal misrepair resulting in cell death, or a viable misrepair resulting in cell mutation.

Two methods of creating lethal lesions are commonly considered. Those created through unrepairable damage and those lethal lesions caused by misrepairs created from interactions of double strand breaks. The direct lethal lesions from unrepairable damage is dependent upon the total dose imparted to the DNA. In contrast the non-lethal lesions undergo repair. The DNA can either repair correctly or misrepair, and this is dependent upon the number of broken ends that can interact; therefore, this mechanism of killing cells is dependent upon the distribution of dose in time. The effects of a double strand break upon the cell survivability have been modeled using a linear-quadratic relationship (Sachs 1997). The linear-quadratic

model accounts for the killing mechanisms and several attempts have been made to fit parameters in the model to actual clinical data (Wang 2003).

1.5. Literature Review

The most complete report describing dosimetry as applied to brachytherapy treatment is the AAPM report number 51 (Nath 1995). The AAPM report discusses practical approaches to achieve accurate dosimetry for brachytherapy sources. It discusses the characteristics of currently (as of 1995) available brachytherapy sources, and contains recommended methods for calculating dose rates for both a point source in one dimension (radial) and a finite cylinder in two dimensions (radial and angular). Potential dosimetry problems are identified, including using inappropriate standards. It also discusses methods of choosing standards and how to recalculate data based upon old standards after a change has occured.

In 1995 Brenner studied the linear quadratic model describing the relationship between radiation dose and cell survivability. He noted that the simple linear quadratic model incorporates sublethal damage repair and repopulation, but it lacked any parameters for the description of the other two 'R's of radiation cellular survival: cell cycle redistribution and reoxygenization. Cell cycle distribution is defined as the proportion of cells in a given phase of their cell growth cycle. Cell cycle redistribution is the new distribution created by a radiation field preferentially killing

cells in certain phases, while preferentially sparing cells in other phases. Reoxygenization is a phenomenon that occurs because certain cells are starved for oxygen (hypoxic), whereas other cells are rich in their oxygen levels. Radiation preferentially kills the cells that are rich in oxygen allowing the hypoxic cells to have access to oxygen; thereby, allowing them to reoxyegenate and increase their sensitivity to radiation. Brenner proposed a more accurate model that would account for these other two parameters: the LQR model, or linear quadratic with incorporation of 'R's. Brenner added a Gaussian term with a specific deviation that changes to account for new distributions in cell cycle and oxygenization as a function of energy deposition.

Many people have spent a lot of time studying the dose distributions resulting from point sources of various isotopes. Most of these studies are performed using Monte Carlo computer codes.

In 1996 Nahum was interested in studying the effects of several beta emitting sources (^{67}Cu, ^{131}I, ^{186}Re, ^{32}P, ^{188}Re, and ^{90}Y) on what he calls tumor control probability. The tumor control probability is defined as the negative exponential of the survival fraction. The survival fraction can be based upon the linear quadratic equation, or in this case Nahum uses only the linear term. Nahum performed his simulations using the Monte Carlo code ETRAN, and modeled his sources in an infinite medium of water.

Also in 1996 Chen modeled many other beta emitting sources (^{3}H, ^{14}C, ^{32}P, ^{35}S, ^{90}Sr, ^{90}Y, ^{106}Ru, and ^{131}I). Chen was more interested in determining microdosimetry dose distributions, rather than modeling survival effects. These calculations were based upon data produced from a Monte Carlo code with an unspecified name.

In 1998 Mainegra studied the dose constants resulting from several isotopes that are used in brachytherapy (^{125}I, ^{103}Pd, ^{169}Yb, and ^{192}Ir). Mainegra focused his modeling on specific brachytherapy seed models in use. He used the EGS4 Monte Carlo code for his computer simulations, compared his simulations to data collected from phantoms, found agreement within 1.5%.

In 2002 Asenjo decided to model ^{90}Sr-^{90}Y brachytherapy seeds. The dose distributions were simulated by the Monte Carlo code PENELOPE. The results of the PENELOPE code were then compared to the ITS3 and EGS4 computer codes. It was found that PENELOPE result lies between the results generated from ITS3 and EGS4.

Whereas some researchers were interested in dose distributions, and the ability to computationally reproduce experimental data, other people were interested in relating the actual effects of radiation damage to biological effects.

In 1997 Sachs reviewed the evolution of modeling the biological response to radiation dose. Sachs begins by discussing double strand breaks and how they can directly cause the death of a cell when undergoing misrepair. He reviews a rate equation describing double strand breaks as a function of dose rate. Since not all double strand breaks lead to the death of the cell, another equation is derived describing the relation between double strand breaks and lethal lesions. The number of lethal lesions is directly related to the natural logarithm of the survival fraction. From this the linear quadratic equation is derived with the linear term dependent upon the single-track lesion kinetics, and the quadratic term dependent upon two-track lesion kinetics. Also included in the quadratic term is a factor that compensates for time delays between the two-track interactions. Sachs also discusses the limitations of the linear quadratic model (without the dose protraction factor); it is inaccurate at high dose rates. A more accurate high dose rate model is the repair-misrepair model. The repair-misrepair model predicts a linear increase in lesions for high doses, whereas the linear quadratic model predicts a quadratic increase. Deviations between the two appear to become significant above about 5 Gy.

In 2003 Wang studied the parameters used in the linear quadratic model by fitting the model to clinical data of irradiated prostate tumors. Wang assumes that the radiation from external beams, and ^{125}I and ^{103}Pd brachytherapy sources all behave in the same manner in damaging prostate tumor cells. This study arose because many

people have been trying to determine the optimum parameters for the linear quadratic formula by fitting clinical data, but have been getting vastly different numbers. Wang suggests the discrepancies arise because earlier studies neglected repopulation effects when analyzing the clinical data. There comes a point when the brachytherapy seed dose rate becomes low enough such that repopulation takes over and the seed no longer has a net killing effect. The dose delivered by the seed before repopulation dominates the killing rate is known as the *effective dose*. The *effective dose* divided by the total dose is the *effective dose fraction*. The effective dose is the dose parameter on which the linear quadratic equation is based. Wang proposed the following values for the linear quadratic model applied to prostate brachytherapy: $\alpha = 0.15 \pm 0.04\ Gy^{-1}$, $\alpha/\beta = 3.1 \pm 0.5$ Gy, and $0 \leq \ln(2)/\lambda \leq 90$ minutes with a 16 minute average value.

Also in 2003 Armpilia studied ^{125}I and ^{103}Pd sources. Just like Wang et al., Armpilia studied the effects of dose upon cellular tissue using the linear quadratic equation with repopulation. The difference between their works is that while Wang was trying to determine the parameter values for prostate tumors, Armpilia was trying to determine what isotopes would be most beneficial to use based solely upon their half-lives.

When modeling brachytherapy sources there are a few more considerations when actually attempting to model the biological effects of treatment.

In 2002 Arnfield considers the fact that when many brachytherapy sources are placed in cancerous tissue there is the potential for sources to move in the tissue. If sources move it is possible that different points in the tissue will receive the same dose, but with differing dose rates and/or dose rate patterns. Arnfield points out that the simple linear quadratic does not account for this (the linear quadratic model does account for this through the use of the 'G' factor). Because of this Arnfield performed an experiment to determine if such a difference in biological reaction does exist, and the results of his experiments did show a difference.

In 2003 Rivard studied the anisotropy of the radiation emitted from a brachytherapy seed. Most studies consider brachytherapy seeds as a uniform source distribution, where in actuality brachytherapy seeds have a significant structure with a source media inside a manufactured casing. Rivard also used superposition to consider the relative importance of different individual sources in the contribution of the overall source for the brachytherapy seed. Rivard found that at large distances the source behaved as an isotropic source, but at short ranges the dose varies significantly with direction from the source. Whether or not this effect plays a significant role in the treatment of cancer is an open question.

The work done leading up to this thesis is intended to promote the development of a computer code that can accurately model the biological effects of

brachytherapy sources. The goal of this code is to provide the medical community with a new tool that goes directly from simulation to biological effect in order to enhance cancer treatment.

1.6. Research Questions

In this thesis, we ask the following questions: What kind of resolution is required to keep the change in dose small over the width of an individual voxel? A voxel is defined as a cube in three-dimensional space in which values such as dose are tallied. What is the effective killing range for particular isotopes involved in brachytherapy (defined here as the radius at which the survival fraction equals 1E-9)? How precise is this range; for example, what is the difference between the killing range and the survival range (defined here as the radius at which the survival fraction equals 1E-7)? How do the shapes of the isodose curves correspond to the isosurvival curves? How do small errors in the placement of brachytherapy seeds affect the overall shape of the survival and dose curves in the vicinity of the deviation?

1.7. Remainder of Thesis

Chapter 2 discusses the methodology that was used to solve the questions proposed in this chapter. It discusses the software used to simulate radiation transport, and the equations used to translate the energy depositions from the simulation into

initial dose rate and cell survival fraction. Also introduced is a simple shielding model that can be used to predict the shape and trends of the cell survival fraction curve.

Chapter 3 presents the results of parametric studies performed on the simple shielding model, as well as comparing the shapes of dose and cell survival fraction curves. Also considered in this section are the effects of sources within close proximity of each other. Several isotopes are simulated using a Monte Carlo radiation transport program to show the effects of a brachytherapy source in cancerous tissue.

Chapter 4 summarizes the results of chapter 3, and uses the results to answer the research questions posed in this thesis. Also included in chapter 4 are recommendations for future work.

2. Methods

2.1. Monte Carlo

2.1.1. Monte Carlo Method

The core of this thesis is modeling radiation transport using the Monte Carlo method. Monte Carlo radiation transport is uses random numbers to simulate the behavior of particles in a real physical system. A sample Monte Carlo particle transport algorithm is shown in Chapter 1 (Figure 1-2).

2.1.2. Monte Carlo Codes

Many Monte Carlo codes are in existence. The ones mentioned in the literature review include PITS, EGS, ITS, and PENELOPE. The two that will be discussed in this section are MCNP and PENELOPE.

MCNP (Monte Carlo N-Particle) was developed at Los Alamos to be a general purpose Monte Carlo code (Briesmeister 2000) and is the most common Monte Carlo code used in the nuclear industry. MCNP allows the user to simulate radiation flowing through geometries specified by the user and has cross section

databases for many different isotopes of interest. It simulates the transport of neutrons, photons and electrons. In addition, MCNP supports detailed source shapes and energy distributions, as well as several different tally types (surface flux, volume flux, heating tallies, etc.). MCNP is a well-developed general use Monte Carlo code.

PENELOPE 2001 (PENetration and Energy Loss of Positrons and Electrons) (Salvat 2001). It was created by Francesc Salvat, Jose M. Fernandez-Varea, Eduardo Acosta, and Josep Sempau. It is comprised of several sets of subroutines that calculate the distance traveled by particles in a given medium, the energy change due to a collision, the generation of secondary particles, and the change in direction of the particle after suffering a collision. The PENELOPE routines support transport of photons, electrons, and positrons. PENELOPE supports fewer materials than MCNP, but PENELOPE has the advantage of being able to transport beta particles down to energies of 100 eV as opposed to MCNP's cutoff of 1 keV.

PENELOPE is a physics engine, and the user can provide his/her own code to create a complete transport simulation. This allows the user to generate a Monte Carlo simulation unique to his/her own problem of interest, but requires the user to write many lines of code. PENELOPE was the Monte Carlo code employed to perform the calculations for this thesis.

2.1.3. Source Definitions

The source sampling routines written for this thesis model a wide variety of energy distributions, source positions, angular distributions, particle types, and spatial distribution. Multiple general sources can be specified. This allows the code to faithfully reproduce emission spectra for complicated decay schemes involving electrons, positrons, and photons.

2.1.4. Tally Definitions

The tally routines used in this project calculate energy imparted, average lineal energy, and absorbed dose, as well as probability distribution spectra for each. Currently only three tally volumes are available to the user: spheres, spherical shells, and voxels. The previously mentioned tallies are calculated only in the entire region of interest for voxel meshes. Tallies inside the individual voxel cells include: absorbed dose per track, energy deposited per track, relative error in energy deposited, initial dose rate, and cell survival fraction.

2.1.5. Material Regions

The current version of the user code supports only an infinite medium of water. Future plans include implementing user code to allow for transport in voxel representations of biological phantoms with a variety of overlay geometries.

2.1.6. Physics

Charged particle transport via Monte Carlo is a challenging physics problem. Charged particles are affected by Coulomb forces surrounding the electron clouds and nuclei in matter and are subjected to continual interactions even without direct collisions. This causes the electrons to undergo thousands of more interactions per track length than uncharged particles.

PENELOPE differs from MCNP in the way it simulates electron transport. MCNP treats electron interactions using multiple scattering theory (Briesmeister 2000), in which groups of interactions are treated as individual interactions. Multiple scattering theory is valid only if the track steps are long enough to encompass many interactions, but short enough to keep energy loss per step low. The calculation is more accurate if the angular deflection per step is small. MCNP implements multiple scattering theory in two parts: energy loss and step length are determined at the step level, and then the step is broken down into substeps and the angular deflections and secondary particle generation from interactions are calculated (Briesmeister 2000).

PENELOPE uses a mixed scheme for particle transport (Salvat 2001). Energy loss and angular deflection cutoffs are specified for the material type. PENELOPE uses these cutoffs as a differentiation between hard and soft interactions. Hard

interactions are interactions that involve a large energy change (above the cutoff) or large direction change. Soft interactions are interactions that happen below the cutoffs. Soft interactions are treated in a manner similar to MCNP's electron transport. Multiple scattering theory is applied to calculate the step length, energy and direction of the particle, and the generation of secondary particles. For soft interactions, PENELOPE uses a random hinge calculation, as opposed to the step/substep method employed by MCNP. For hard events, PENELOPE performs a detailed simulation of the individual interactions. This process yields more accurate spatial distributions of scattering, and tracks the particles near interfaces more accurately, but is also more computationally expensive than multiple scattering theory. PENELOPE allows the user to adjust the tradeoffs between accuracy and speed by changing the cutoff values.

PENELOPE also has the ability to track positrons and electrons down to energies of 100 eV (as opposed to 1 keV for MCNP), making PENELOPE advantageous to use in microdosimetry applications or for transport of low energy beta sources.

2.2. Linear Quadratic Formula

The linear quadratic equation for cell survival fraction is (Sachs 1997):

$$S = e^{-(\alpha D + \beta G D^2)}, \tag{2-1}$$

where S is the survival fraction of a cell within the volume of a given voxel cell (*unitless*), D is the total dose delivered to a given voxel cell (Gy), G is the dose protraction factor that accounts for damage repair and depends on the temporal pattern of dose delivery (*unitless*), and α (Gy^{-1}) and β (Gy^{-2}) are fitting parameters based upon the type of cell, and type of radiation. In this equation the 'G' factor is a modifying parameter of the squared dose term, and accounts for the time difference between particles emitted by the radionuclide hitting a given cell multiple times.

The linear quadratic equation is dependent upon three tissue specific parameters: the linear lesion coefficient (α), the quadratic lesion coefficient (β), and the tissue repair half-time (τ). The values calculated by Wang (Wang 2003) were used throughout this thesis $\alpha = 0.15 \pm 0.04\ Gy^{-1}$, $\alpha/\beta = 3.1 \pm 0.5\ Gy$, and $0 \leq \tau \leq 90$ minutes with a best estimate of 16 minutes. The linear lesion coefficient represents the number of lethal lesions imparted to the DNA per unit of dose. The quadratic lesion coefficient represents the interactions of these potentially lethal lesions and has units of inverse dose squared. The half-time for damage repair characterizes the rate at which cells remove potentially lethal double strand breaks. The rate of DNA damage repair (λ) is related to the repair half-time by the following equation:

$$\lambda = \frac{\ln(2)}{\tau}. \tag{2-2}$$

An important quantity used in the linear quadratic equation is the dose protraction factor (G). The dose protraction factor accounts for the temporal distribution of dose. It is a result of the repair processes that repair damage to the DNA. This 'G' factor is defined as (Sachs 1997):

$$G = \left(\frac{2}{D^2}\right)\int_{-\infty}^{\infty} \dot{D}(t)dt \int_{-\infty}^{t} e^{-\lambda(t-t')}\dot{D}(t')dt', \tag{2-3}$$

where G is the time dependent parameter for the cell survival equation (*unitless*), D is the total dose (Gy), $\dot{D}(t)$ is the instantaneous dose rate (Gy/hr), λ is the biological time constant (hr^{-1}), and t is time (hr). For an exponential decay over infinite time and no repopulation, this reduces to:

$$G = \frac{k}{k+\lambda} = \frac{\frac{\ln(2)}{t_{1/2}}}{\frac{\ln(2)}{t_{1/2}} + \frac{\ln(2)}{\tau}}, \tag{2-4}$$

where k is the radionuclide decay time constant (hr^{-1}), $t_{1/2}$ is the radionuclide half-life (hr), λ is the biological repair time constant (hr^{-1}), and τ is the tissue repair half-time

(*hr*). As the radionuclide half-life becomes very long, $t_{1/2}$ becomes large and G approaches 0. If the radionuclide half-life becomes very short, $t_{1/2}$ becomes small and G approaches 1. For a pulse of radiation (square wave), G reduces to:

$$G = \frac{2}{(\lambda t)^2}\left(e^{-\lambda t} - 1 + \lambda t\right), \tag{2-5}$$

where λ is the biological repair time constant (hr^{-1}) and t is the width of the pulse (*hr*). As the pulse width (*t)* becomes long, dose is delivered slowly and G approaches 0. If the pulse width becomes very short, dose is delivered very quickly and G approaches 1.

2.3. Assumptions

To study the shapes of dose and cell survival curves, several important assumptions were made. One assumption is that the property of superposition holds for the system being studied. The use of superposition allows the dose curves calculated from a single source to be used to construct the dose and survival curves for multiple sources. Also assumed is that repopulation effects are negligible. Cells will regrow at a certain rate, and the net killing rate will be the difference between the total killing rate and the regrowth rate. Because repopulation effects are ignored, the cell killing probability will be less than estimated, and the amount of radiation dose

required to create the desired effect will be underestimated. Another assumption is that cellular tissue can be accurately modeled as water. This assumption is based upon the reasoning that cellular tissues are composed mostly of water. More complex treatment of tissue (spatially varying cross-sections and densities) may be incorporated in future studies.

2.4. Calculations

To answer the research questions posed in this thesis, we must create a piece of software that can calculate the cell survival fraction field for typical brachytherapy sources and seeding patterns. First the tally region is discretized using a cubic mesh. Energy deposits are tallied in the individual voxel cells and are normalized per track. Absorbed dose is calculated from

$$D_T = \frac{\varepsilon}{m}, \tag{2-6}$$

Here D_T is the dose per track in a given voxel cell (Gy), ε is the average energy deposited in the given voxel cell per track (J), and m is the mass of the voxel cell (kg). This dose is multiplied by the total activity of the sources to find the initial dose rate:

$$\dot{D}_0 = A_0 N_s D_T, \tag{2-7}$$

where $\dot{D}_0$ is the initial dose rate in a given voxel cell (*Gy/hr*), A_0 is the initial activity of a source (*Bq/hr*), N_s is the number of sources (sum of all the source weights), and D_T is the dose per track in a given voxel cell (*Gy/Bq*). Because brachytherapy uses permanent radioisotope implants, it is assumed that the instantaneous dose rate decays exponentially with time:

$$\dot{D} = \dot{D}_0 e^{-kt}, \tag{2-8}$$

where D is the instantaneous dose rate in a given voxel cell (*Gy/hr*), D_0 is the initial dose rate in a given voxel cell (*Gy/hr*), k is the decay constant for the particular isotope being used (hr^{-1}), and t is the elapsed time (*hr*). The total dose delivered in the voxel is:

$$D = \int_0^\infty \dot{D}(t)dt = \int_0^\infty \dot{D}_0 e^{-kt} dt = \frac{\dot{D}_0}{k}, \tag{2-9}$$

where D is the total dose delivered to the given voxel cell (*Gy*), *D(t)* is the instantaneous dose rate to the given voxel cell (*Gy/hr*), $\dot{D}_0$ is the initial dose rate to the voxel cell (*Gy/hr*), k is the decay constant for the isotope of the radionuclide being used (hr^{-1}), and t is the time elapsed since implantation (*hr*). In this thesis

repopulation is ignored. If repopulation were to be considered the integral would be from 0 to t, where t would be the effective treatment time. The effective treatment time is defined as the time at which the cellular repopulation rate equals the cellular destruction rate. Substituting this into the cell survival fraction equation (Eq. 2-1); the following equation is obtained:

$$S = e^{-\left(\frac{\alpha}{k}\dot{D}_0 + \frac{\beta}{k(k+\lambda)}\dot{D}_0^2\right)}, \tag{2-10}$$

where S is the tissue cell survival fraction in the voxel cell (*unitless*), D_0 is the initial dose rate (*Gy/hr*), k is the radionuclide decay constant (hr^{-1}), λ is the biological decay constant (hr^{-1}), and $\alpha\,(Gy^{-1})$ and $\beta\,(Gy^{-2})$ are fitting parameters. S is calculated for each voxel cell and is visualized to show the effective 'kill' radii.

2.5. Effective Kill Range

When a radioisotope point source is emitting radiation in a uniform medium, the following equation approximates the dose rate as a function of radial distance from the source,

$$\dot{D} = \frac{Xe^{-\mu R}}{R^2}. \tag{2-11}$$

Here $\dot{D}$ (Gy/hr) is the dose rate at the distance R (cm) in the media, X $(Gy*cm^2/hr)$ is a constant dependent upon the source strength, and μ (cm^{-1}) is the linear attenuation coefficient which is dependent upon particle energy and the media surrounding the source.

When dose rate is evaluated in this manner it can be used to investigate (see Equation 2-10) the general trends of cell survival fraction as a function of distance from the source. Varying parameters in the simplified model allows one to study their effect on dose and cell survival curves. This can also be used to perform a simplistic study of the *damage region*. The damage region is defined as the difference between the survival radius (cell survival fraction = 10^{-7}), and the kill radius (cell survival fraction = 10^{-9}).

2.6. Superposition

After running several test simulations it was found that the time required to simulate one point source was prohibitive, (several days to a week) to generate a solution with good statistics. Because brachytherapy requires the use of hundreds of sources, another method was devised to solve the multiple-source problem within a reasonable amount of time. It is assumed that the radiation field in a region near two different radioactive sources is merely the sum of the individual radiation fields. The

dose fields will be superimposed and the survival field recalculated. The applicability of superposition will be tested later in this thesis.

2.7. Supporting Programs

Several different programs were written to analyze the data calculated by the main code. Data calculated for a single source is replicated in an array of structured sources using superposition. The dose is calculated by interpolating the dose at voxel tally centers in the overlapping regions of the voxel mesh. Another code takes the output of the main program, combines the voxels at equivalent radii from the source and averages them together for easy visualization.

3. Results

3.1. Introduction

In the following subsections, the results of the studies performed on dose and cell survival fraction of specific radioactive point sources (^{103}Pd, ^{137}Cs, ^{90}Sr, and ^{125}I) are presented. This chapter begins by developing approximate single source dose and cell survival fraction distributions to perform parametric studies. Then the effects of a second source are investigated. The second source is placed a known distance away and superimposed upon the calculation from the first source. The effect of the second source upon the cell survival fraction as the sources are moved closer together is observed. Finally the effects of modifying the parameters defining the source are studied to determine their impact upon the cell kill radius (radius from the source at which the cell survival fraction is 5%).

In the next section, the dose and cell survival distribution of two isotopes commonly used in brachytherapy (^{103}Pd and ^{125}I), and two other isotopes (^{137}Cs and ^{90}Sr) are analyzed. These sources are studied using data generated from the PENELOPE Monte Carlo code. Individual point sources are simulated in an infinite medium of water, and the shape of the dose and cell survival fraction curves are examined for each isotope. Also observed is the effect of separation distance of two identical sources on dose and cell survival fraction.

Data generated for the dose and cell survival fraction distributions are used as input data for three dimensional visualization. First an individual point source of each isotope is plotted (cell survival fraction) to compare the relative killing power of each isotope. Then for visualization purposes, an array of sources is generated to form a theoretical brachytherapy seed loading in cancerous tissue.

Also investigated is the applicability of the superposition assumption simulating a ^{3}H point source's dose curves superimposed upon each other (and cell survival fraction recalculated from the new dose curve) compared to a direct simulation of multiple ^{3}H sources.

3.2. Preliminary Studies

This section describes a simple point source shielding model, which is used to approximate the detailed transport solution generated by the PENELOPE code. The purpose of this model is to perform parametric studies of effects of different parameters (source strength, shielding material, isotope dependence, and biological properties) upon changes in dose and cell survival fraction. Of particular interest is the *kill radius* (the radius at which the survival fraction equals 1E-9), *survival radius* (the radius at which the survival fraction equals 1E-7), and the *damage region* (the difference between the survival and kill radii).

3.2.1. Dose and Survival Radius Comparison

To investigate the expected shape of the dose curves, both Equation 2-10, and 2-11 were used with the values listed in Table 3-1 to calculate the radial dose and cell survival fraction curves for a particular point source. The particular values chosen were selected because they are representative of the conditions of the simulations shown later in this chapter.

Name	Variable	Initial Value	Units
Intensity	X	1	$Gy*cm^2/hr$
Attenuation	μ	1	cm^{-1}
Linear Lesion Coefficient	α	0.15	Gy^{-1}
Quadratic Lesion Coefficient	β	0.048	Gy^{-2}
Isotope Decay Constant	k	0.0017	hr^{-1}
Rate of DNA damage repair	λ	2.60	hr^{-1}

Table 3-1. Initial Values for the Simple Point Source.

The dose rate is the amount of energy imparted per unit mass of the absorbing material. This is important because more energy imparted to a cell decreases its chance of survival. The radial dose rate curve is often modeled as the product of an exponential decay (due to attenuation), and a $1/R^2$ function (due to geometric attenuation).

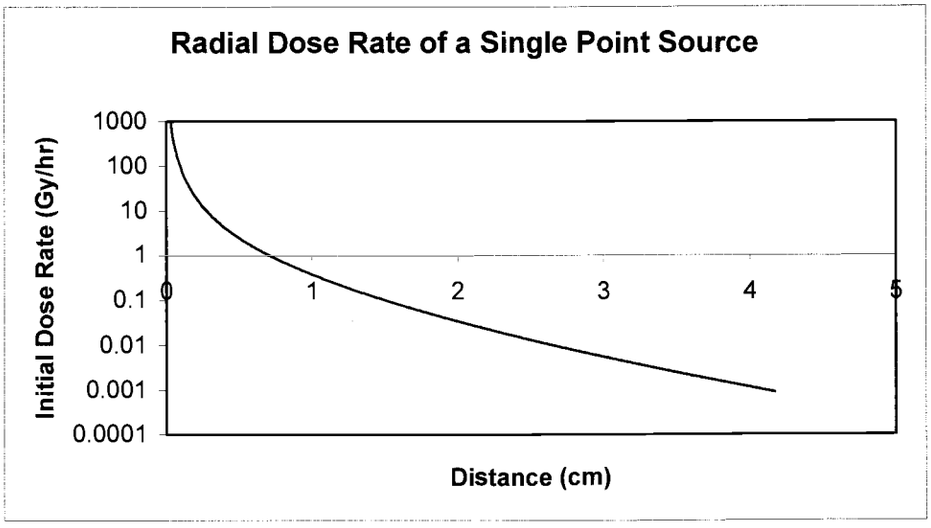

Figure 3-1. Radial Dose Rate of a Single Point Source.

Near the source, the $1/R^2$ term is dominant (very large) compared to the exponential term (close to one). Further away from the source the curve approaches that of an exponential decay as shown in Figure 3-1.

The next graph to be examined is the radial cell survival fraction. It is expected that the shape of this curve will be very close to 0% survival near the source where the dose is high and significant damage is done to the cells. As the distance from the source increases, the cell survival fraction should increase to 100%, as the cells are protected by sufficient shielding.

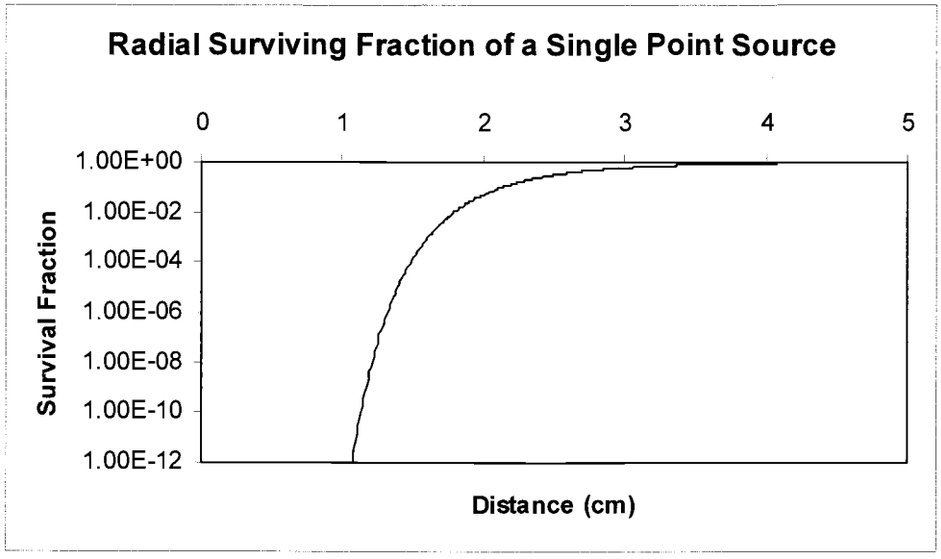

Figure 3-2. Radial Surviving Fraction of a Single Point Source.

Figure 3-2 shows the cell survival fraction for this sample problem, and it is seen that it is effectively zero at small distances from the source. Further away from the source the cell survival fraction increases rapidly approaching 100% survival. The region of the curve where the survival fraction is between 1E-9, and 100% is interesting, because in this region cells are exposed to the effects of radiation, but are not being completely killed. In this region there is potential for radiation induced mutations and/or surviving tumor cells.

3.2.2. Two Source Studies

In this section, the simple shielding model and superposition are used to model the effects of survival fraction upon the distance between two identical

sources. The data used for this calculation are shown in Table 3-2. These values are the same as those used in the computational simulations presented later in this thesis.

Name	Variable	Initial Value	Units
Intensity	X	1	$Gy*cm^2/hr$
Attenuation	μ	1	cm^{-1}
Linear Lesion Coefficient	α	0.15	Gy^{-1}
Quadratic Lesion Coefficient	β	0.048	Gy^{-2}
Isotope Decay Constant	k	0.0017	hr^{-1}
Rate of DNA damage repair	λ	2.60	hr^{-1}

Table 3-2. Initial Values for Two Source Studies.

In the limit as the two sources are placed large distances apart, the dose and cell survival curves will not overlap, i.e. the sources do not see each other. As the sources are placed closer, the dose curves from each source will overlap. This is particularly significant in the region where there is a sharp rise in the survival fraction. When the sources have a very small spacing, the cell survival fraction continues to drop until effectively every cell is killed.

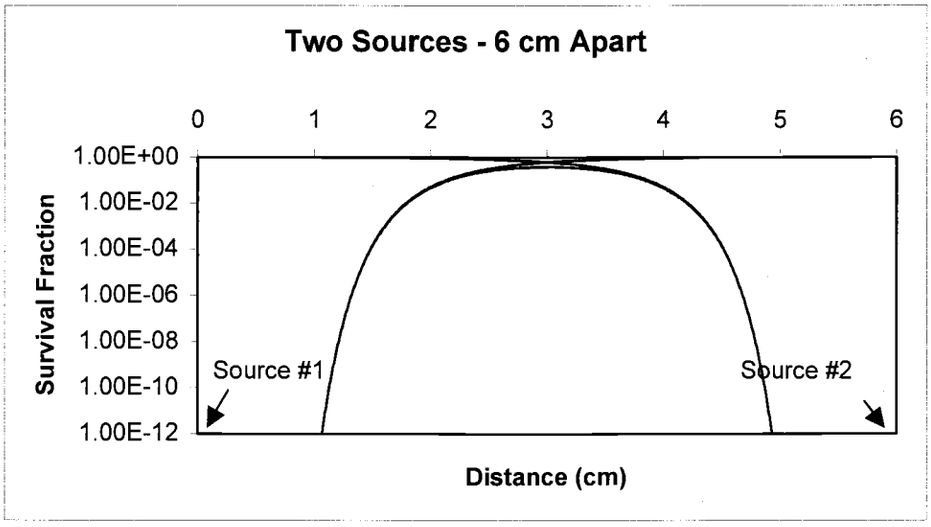

Figure 3-3. Two Sources Studies – 6 cm Separation Distance.

At 6 cm separation (see Figure 3-3), the individual sources do not see each other. At this range the two sources kill in their local zones and do not interact at all.

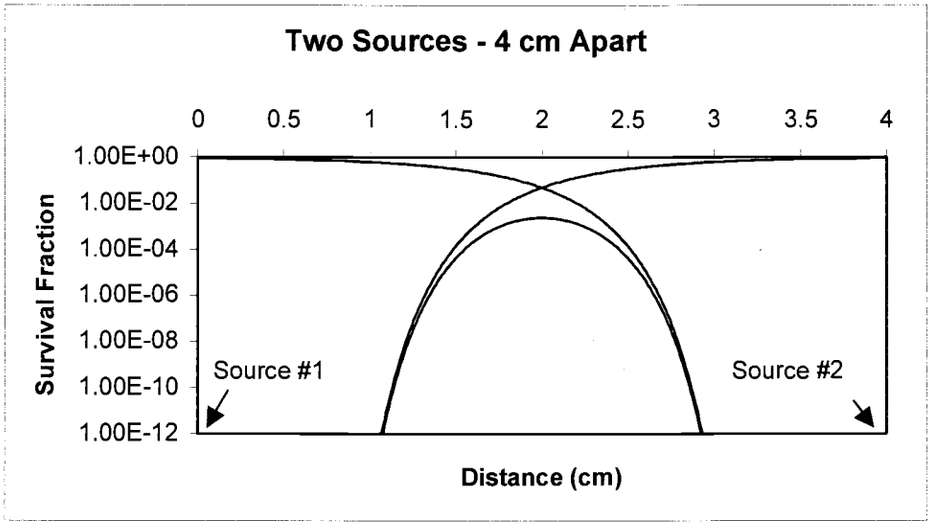

Figure 3-4. Two Source Studies – 4 cm Separation Distance.

Figure 3-4 shows that at 4 cm separation, there is significant overlap at the tail end of the two dose curves, but the survival fraction still looks strongly like that of two independent sources.

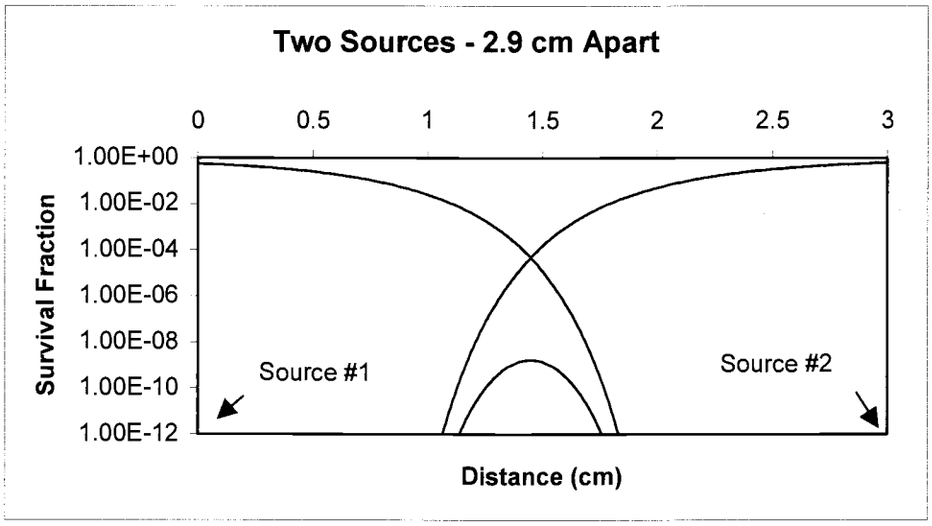

Figure 3-5. Two Source Studies – 2.9 cm Separation Distance.

At 2.9 cm (see Figure 3-5), there is enough of an overlap between the two sources to effectively destroy all cells between the two sources. The cell survival fraction curve remains below 1E-9. If the spacing between the two sources was further decreased, the height of the cell survival curve would decrease further.

3.2.3. Parametric Studies of Damage Region

In the following case studies, the kill radius is defined as the 10^{-9} cell survival radius, the survival radius is defined as the 10^{-7} cell survival radius, and the damage

region is defined as the difference between the survival and kill radii. The initial data used for each of these calculations is as shown below in Table 3-3. This data is based upon values similar to those used in the computational simulation later in this chapter.

Name	Variable	Initial Value	Units
Intensity	X	1	$Gy*cm^2/hr$
Attenuation	μ	1	cm^{-1}
Linear Lesion Coefficient	α	0.15	Gy^{-1}
Quadratic Lesion Coefficient	β	0.048	Gy^{-2}
Isotope Decay Constant	k	0.0017	hr^{-1}
Rate of DNA damage repair	λ	2.60	hr^{-1}

Table 3-3. Initial Values for Sensitivity Studies.

The effect of source intensity on the kill and survival radii is presented in Figure 3-6. The intensity of radiation depends on the quantity and half-life of the radionuclide present.

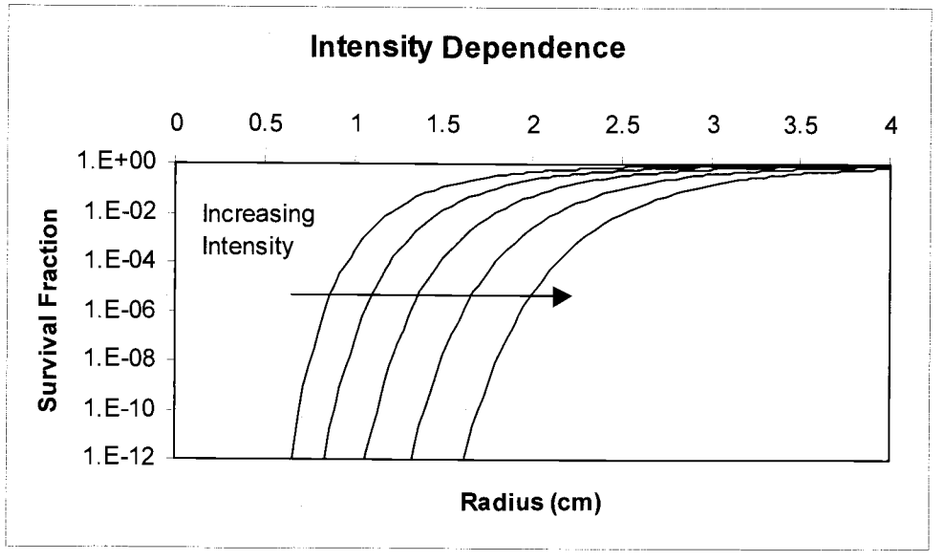

Figure 3-6. Intensity Dependence.

In Figure 3-6 it can be seen that as the intensity of the source increases, the kill radius increases. As the intensity increases, more and more particles are emitted increasing the number of particles (and energy) deposited in cells further away from the source.

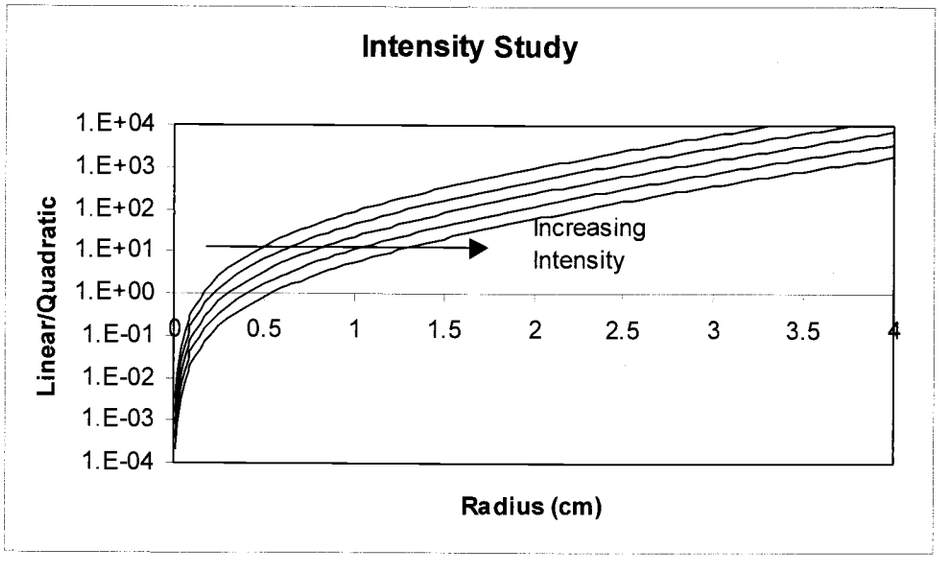

Figure 3-7. Intensity, Ratios of the Linear and Quadratic Terms.

Figure 3-7 shows that at a given radius, an increase in intensity makes the quadratic term more important (linear/quadratic decreases), as would be expected from the D^2 term from the linear quadratic equation.

Figure 3-8 illustrates the effect of the attenuation factor on the survival and kill radii. The attenuation factor is a sensitive function of the material through which the radiation is traveling and the energy of the particle. The density of the material, and the interaction cross-sections (σ) are the important material properties for attenuation.

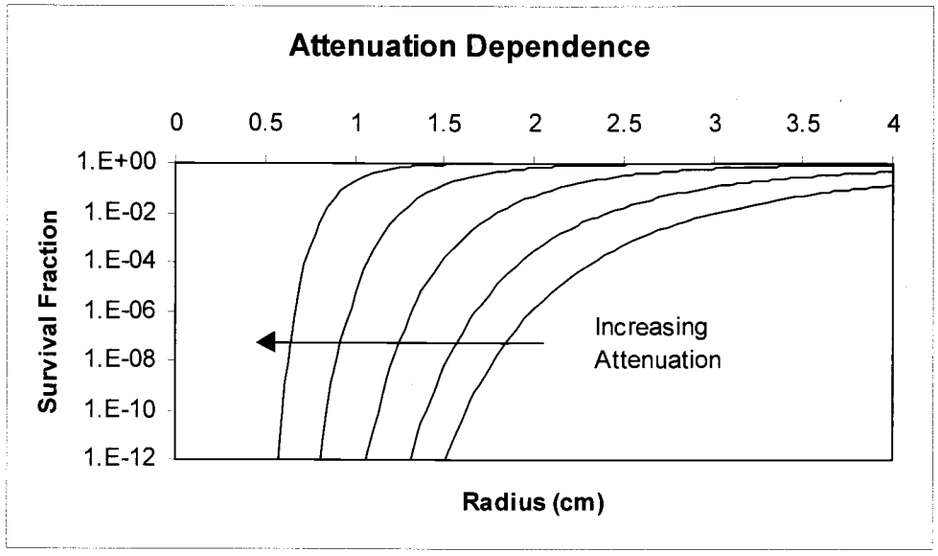

Figure 3-8. Attenuation Dependence.

Physically, it is expected that an increase in attenuation will cause a decrease in kill radius. This model demonstrates that expected behavior.

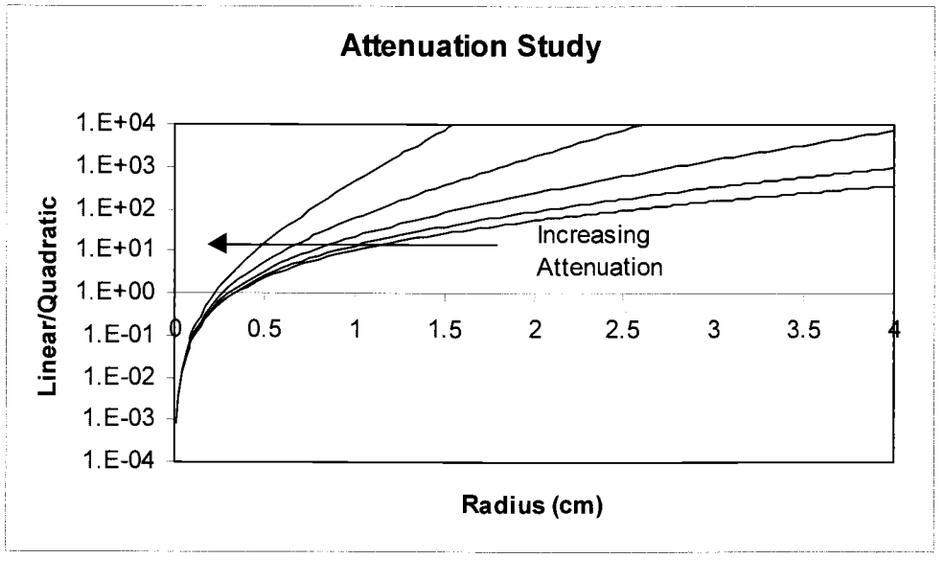

Figure 3-9. Attenuation, Ratios of the Linear and Quadratic Terms.

Figure 3-9 shows that at a given radius, as attenuation increases the quadratic term of the linear quadratic equation becomes less important. This is physically explained because more of the dose is being attenuated and as there is less dose, the D^2 term becomes less important.

The linear lesion coefficient (α) is a biological parameter used to predict the number of fatal lesions produced by one-track action (one particle). It is a function of the type of cell being irradiated and the particle LET (linear energy transfer).

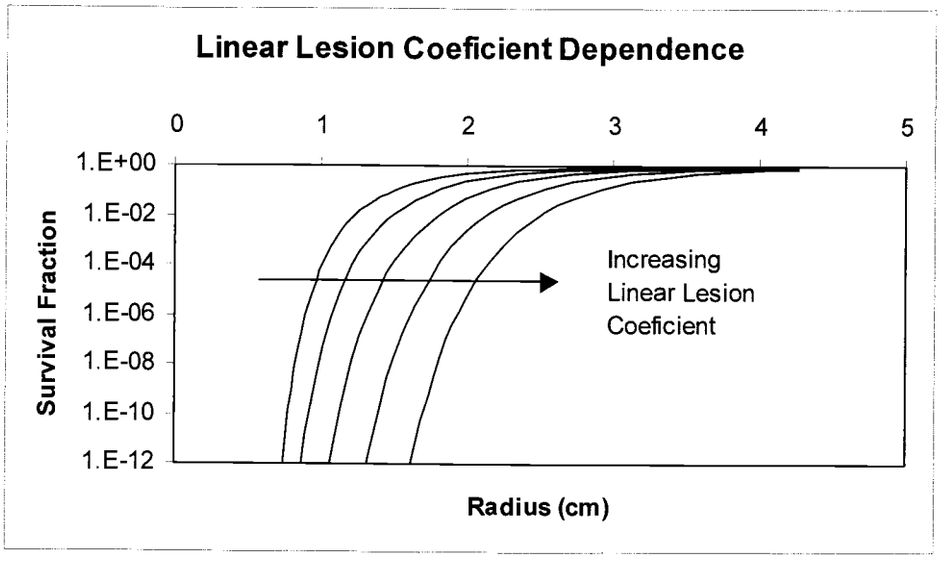

Figure 3-10. Linear Lesion Coefficient Dependence.

A larger linear lesion coefficient physically means that more of the lesions that are a result of one-track action are fatal. More fatal lesions implies that fewer

particles will be required to kill a cell, causing an increase in the kill radius. Figure 3-10 demonstrates this behavior.

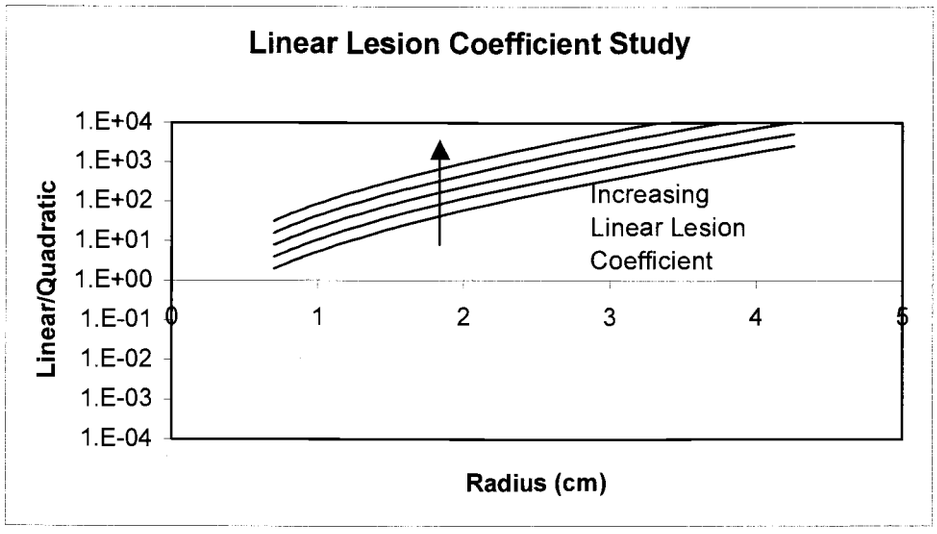

Figure 3-11. α, Ratios of the Linear and Quadratic Terms.

Figure 3-11 shows that at a given radius, as the linear lesion coefficient is increased the quadratic term becomes less important. This is because the linear term is directly proportional to the linear lesion coefficient.

The quadratic lesion coefficient (β) is also a biological parameter that is based upon lesions caused by particle tracks, but it accounts for two-track (two particle) interactions. Just like the linear lesion coefficient, its magnitude is dependent upon the cell type being irradiated and particle LET.

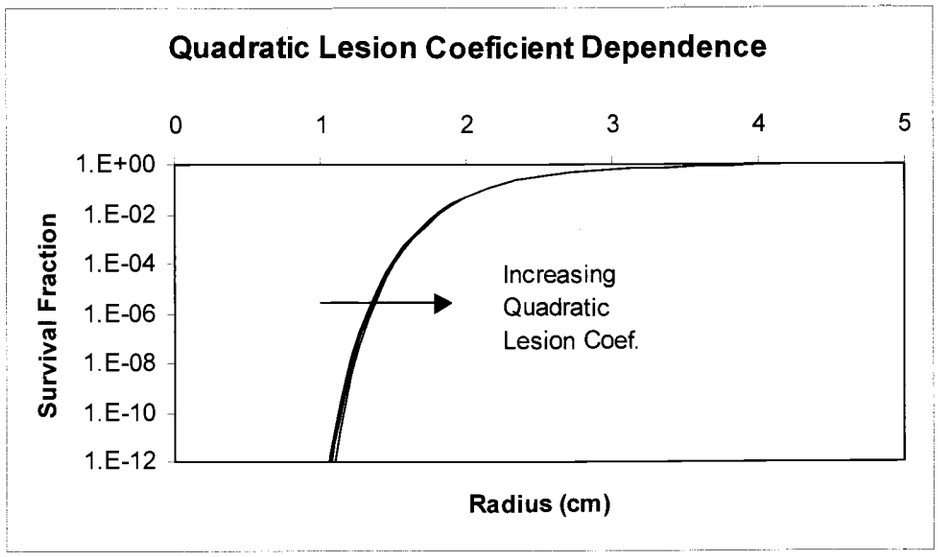

Figure 3-12. Quadratic Lesion Coefficient Dependence.

The quadratic lesion coefficient physically describes the formation of lesions occurring due to interactions between lesions in the DNA. When multiple lesions occur within a short amount of time, the combined effects of several lesions that may be non-lethal by themselves become lethal when occurring together. The more rapidly the radiation is emitted, the more lesions are created which increases the potential of interactions between the lesions. A larger value of β would seem to indicate a greater effect of interactions between lesions and cause an increase in the kill radius as seen in Figure 3-12. However, with the data used in this model it was found that β has a small effect upon the kill radius.

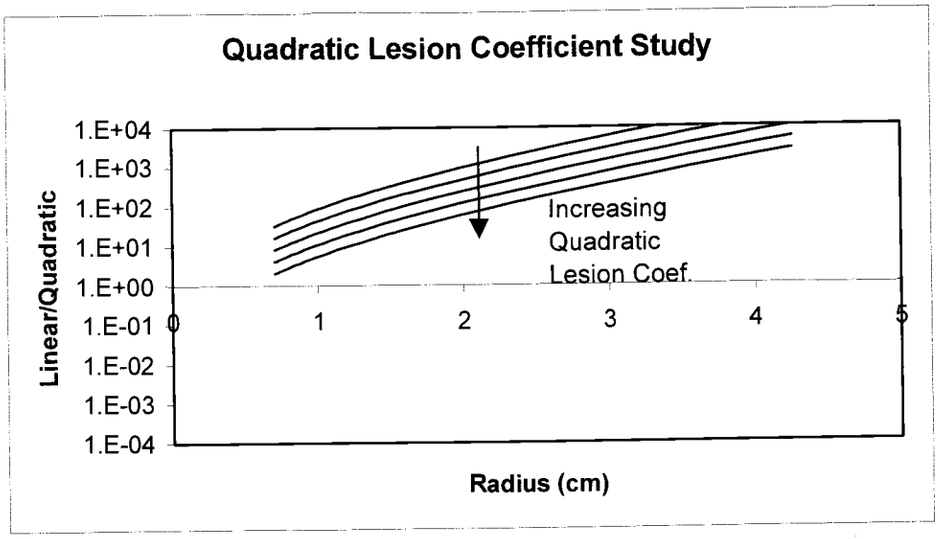

Figure 3-13. β, Ratios of the Linear and Quadratic Terms.

Figure 3-13 shows the effect of increasing the quadratic lesion coefficient on the linear/quadratic ratio. At a given radius, as the quadratic lesion coefficient is increased the quadratic term becomes more important, as would be expected.

Figure 3-14 shows the effect of radionuclide decay constant on kill and survival radius. The isotope decay constant is a function of the specific source nuclide and is equal to $\ln(2)/t_{1/2}$, where $t_{1/2}$ is the isotope's half-life.

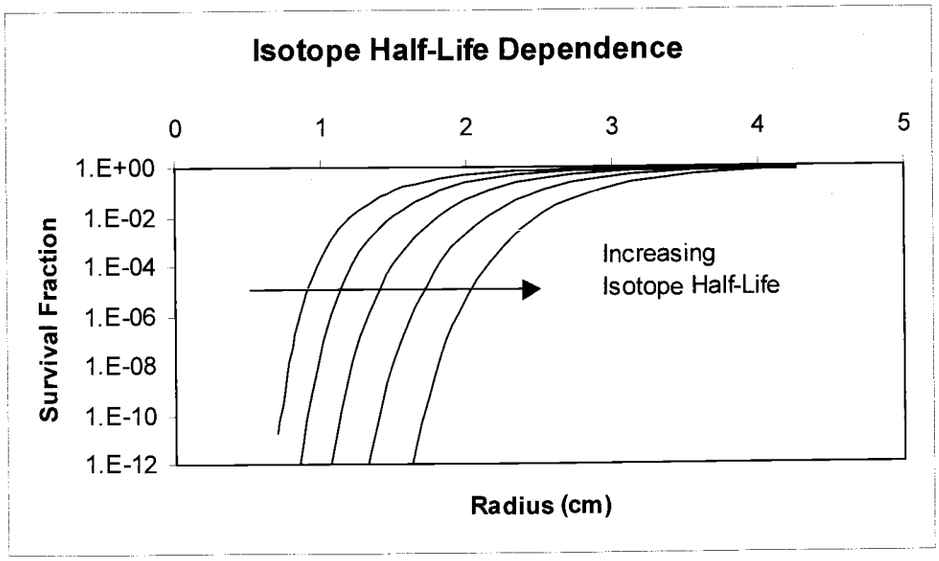

Figure 3-14. Isotopic Half-Life Dependence.

An isotope with a short half-life will decay rapidly and a small quantity would be required to create a source of a given decay rate. This small source quantity will generate a relatively small dose, which decreases the cell killing probability, and the kill radius will decrease. In summary, for a given initial decay rate the isotope decay constant increases, the kill radius will decrease. This behavior is shown in Figure 3-14.

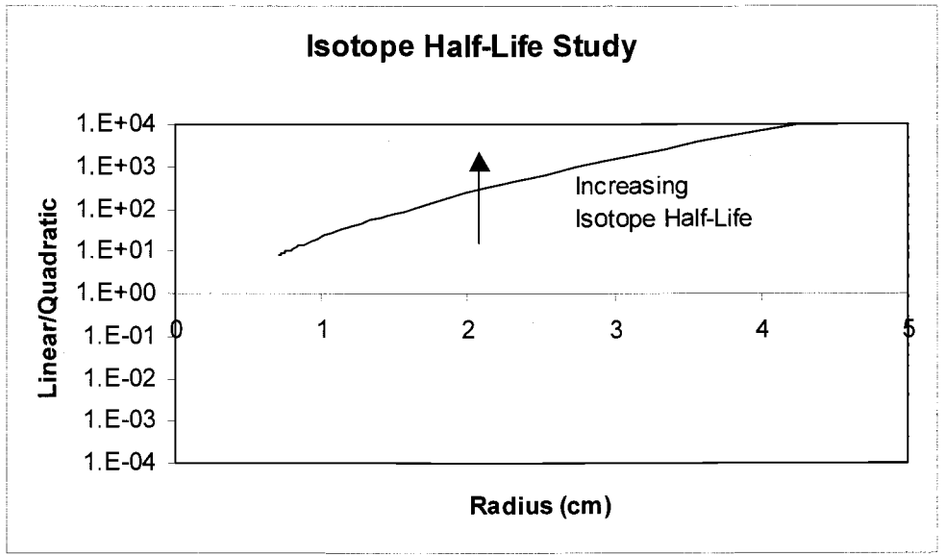

Figure 3-15. Isotope Half-Life, Ratios of the Linear and Quadratic Terms.

Figure 3-15 shows that changing the isotope half-life has no effect on the relative values of the linear and quadratic terms. This is because the sources are normalized to the same initial dose rate and because of this the relative ratio is equal to $\alpha(k+\lambda)/\beta D$. The isotope decay constant is almost always much smaller than the rate of DNA damage repair, therefore k becomes unimportant in changing the ratio.

Figure 3-16 shows the effect of the DNA repair half-time on the kill and survival radii. The rate of DNA damage repair is the rate at which the cell repairs the effects of radiation. The rate of DNA damage repair is related to the DNA repair half-time by $k=\ln(2)/\tau$. The larger the value of the rate of DNA damage repair the more rapidly lesions are repaired.

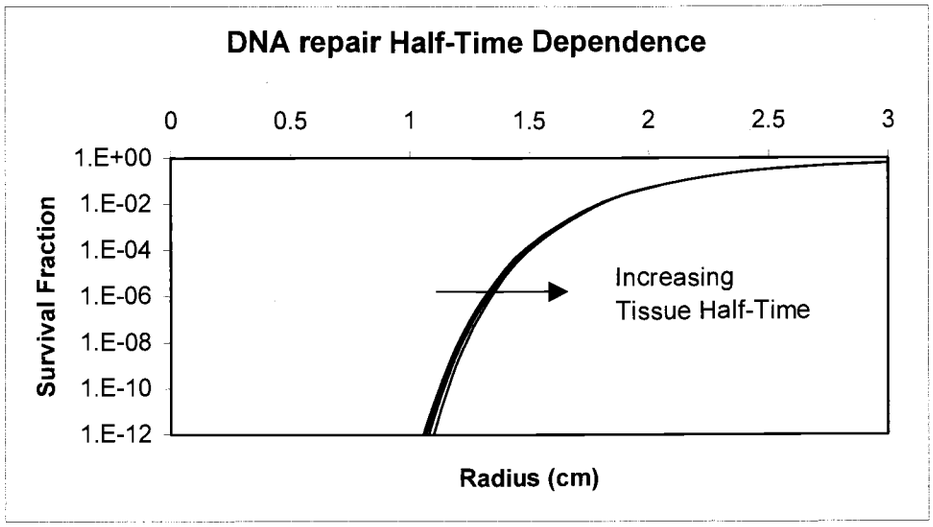

Figure 3-16. DNA repair half-time Dependence.

DNA repair half-time effects are relevant when there is a time delay between radiation doses. For example: when a cell is damaged by two independent particles and multiple non-lethal lesions are created. If these non-lethal lesions are repaired before a large number occur the cell will survive. It was observed previously that the magnitude of the quadratic lesion coefficient did not change the kill or survival radii. For this test problem, the kill and survival radii are relatively insensitive to the tissue decay constant. In general an increase in the tissue decay constant will cause a reduction in the likelihood of multiple particle interactions within the target cell and this can be seen in Figure 3-16. Mathematically this can be explained from Equation 2-10. The quadratic term is proportional to $1/k*(k+\lambda)$, and as λ (rate of DNA damage repair) increases the denominator increases and the value of the quadratic term

decreases. Therefore if λ increases the survival fraction will increase and the kill radius will decrease.

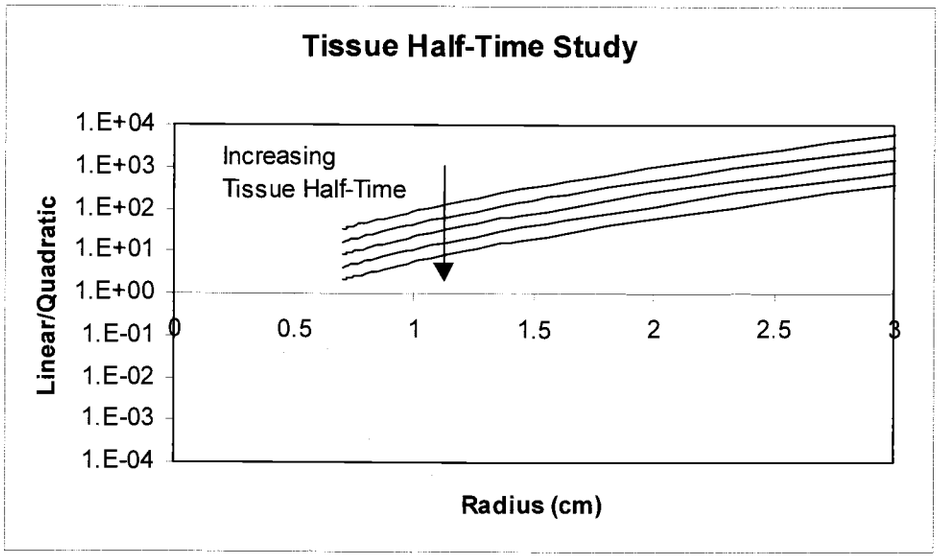

Figure 3-17. DNA repair half-time, Ratios of the Linear and Quadratic Terms.

In Figure 3-17 at a given radius, as the DNA repair half-time is increased the quadratic term becomes more important. This is related to the discussion above about a longer repair time allowing more non-lethal lesions to form, possibly becoming lethal lesions.

3.3. Brachytherapy Radioisotope Source Calculations

The sources that were studied are ^{103}Pd, ^{137}Cs, ^{90}Sr, and ^{125}I. These sources have differing emission spectra and some emit gamma particles, whereas others emit

beta particles. The common factor between all of them is that they are all commonly used in brachytherapy. From the simple shielding studies previously shown, there is a certain expected shape for the dose and survival curves, although they will all be slightly different due to differing emission particle type and energy. Presented in this section are the results for one and two source studies comparing the shapes of the dose and survival curves against each other.

The decay schemes for the isotopes studied are as follows (Martin 2000 and Parrington 1996):

^{103}Pd decays by electron capture ($t_{1/2}$ of 16.99 days) to an isomeric state of ^{103}Rh ($t_{1/2}$ of 56.12 minutes), with the emission of a 357 keV gamma plus the related x-rays. $^{103}Rh^{*}$ is assumed to be in equilibrium with ^{103}Pd, and the ^{103}Rh emits a gamma of 39.8 keV plus the related x-rays. The ground state of ^{103}Rh is stable.

^{125}I ($t_{1/2}$ of 59.4 days) decays by electron capture, with an emission of a gamma (35.5 keV) and the related x-rays to the ground state of ^{125}Te, which is stable.

^{137}Cs has a half-life of 30 years. It decays by beta emission, with a maximum emission energy of 1.18 MeV. The most probable (94%) decay takes ^{137}Cs into the isomeric state of ^{137}Ba. The impact of $^{137}Ba^{*}$ was NOT taken into account during the simulations run for this thesis. The ground state of ^{137}Ba is stable.

^{90}Sr ($t_{1/2}$ of 28.7 years) decays by electron emission (maximum electron energy of 546 KeV) to ^{90}Y ($t_{1/2}$ of 64 hours), and is assumed to be in equilibrium with ^{90}Y. ^{90}Y decays by electron emission to ^{90}Zr (maximum electron energy of 2.28 MeV). One possible branching scenario includes the emission of a gamma, but the probability of emission is on the order of 10^{-11}. This gamma was NOT taken into account, it was considered insignificant. The ground state of ^{90}Zr is stable.

3.3.1. Individual Source Comparison

This section compares the radial shapes of the dose and cell survival fraction curves for a single point source of each isotope. Individual sources are simulated by means of a Monte Carlo program as a point source in an infinite medium of water. Table 3-4 contains the initial parameters used in each simulation.

Isotope	Particle Type	Initial Activity (Ci)	k (hr^{-1})	λ (hr-1)	α (Gy^{-1})	β (Gy^{-2})	Particles Run
^{103}Pd	P	1E-4	1.70E-3	1.5	0.15	0.048	8.34M
^{137}Cs	e^-	1E-4	2.63E-6	1.5	0.15	0.048	15.8M
^{90}Sr	e^-	1E-4	2.75E-6	1.5	0.15	0.048	5.42M
^{125}I	P	1E-4	4.86E-4	1.5	0.15	0.048	6.11M

Table 3-4. Values Used for the Simulation of Brachytherapy Sources.

To compare the four isotopes studied in this thesis the initial dose rate associated with 1 μCi of each source is plotted in Figure 3-18. Of the four isotopes

^{103}Pd and ^{125}I are gamma (photon) emitters, and ^{137}Cs and ^{90}Sr are beta (electron) emitters. An interesting point to note is that ^{90}Sr has a significantly longer half-life (28.8 years) than its daughter product ^{90}Y (2.67 days – ground state), and therefore ^{90}Y is assumed to be in equilibrium with ^{90}Sr. ^{90}Y is also a beta emitter and was taken into account when generating the ^{90}Sr spectrum. ^{103}Pd's decay scheme includes electron capture, which changes ^{103}Pd into an excited state of ^{103}Rh. The half-life of ^{103}Pd (17 days) is significantly larger than that of the excited state of ^{103}Rh (56 minutes); therefore, again equilibrium is assumed and ^{103}Rh is taken into account in the generation of the source spectra of ^{103}Pd (both gamma emitters).

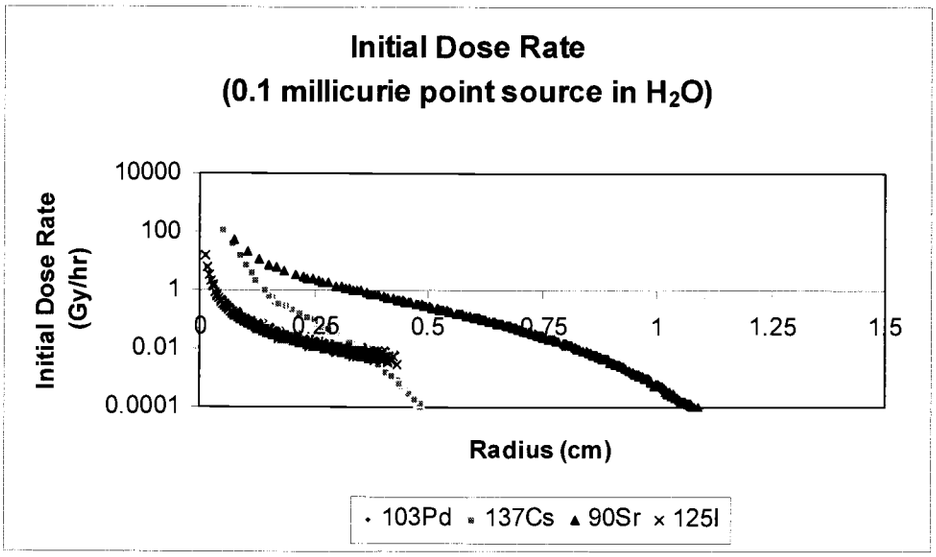

Figure 3-18. Dose Rate – Point Sources.

From Figure 3-18 one can see the relative dose that each source imparts to its surrounding region. The two beta emitters studied impart more dose to the

surrounding material than the two gamma emitters. ^{90}Sr imparts the most dose, followed by ^{137}Cs, then comes ^{103}Pd, and finally ^{125}I, which imparts the least dose of the four isotopes studied. The interesting thing about ^{103}Pd and ^{125}I is the fact that they impart almost the same dose to the surrounding tissue.

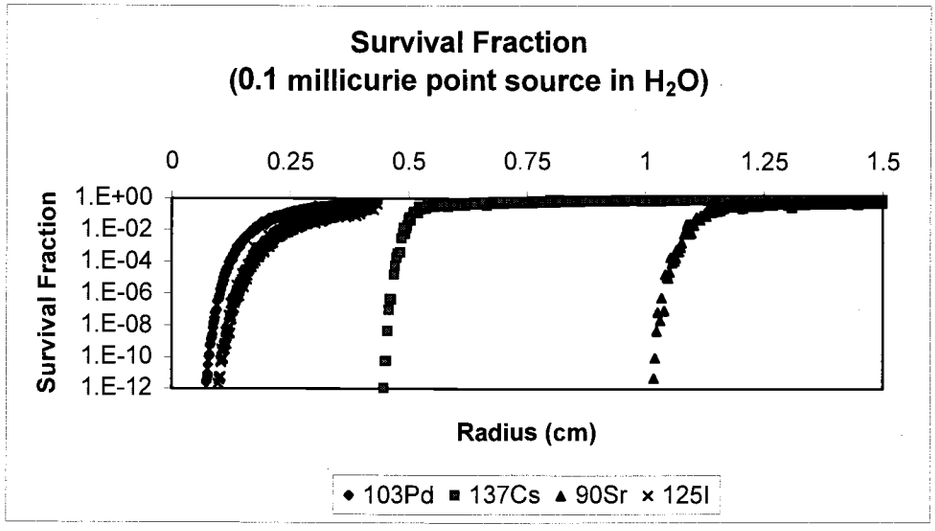

Figure 3-19. Cell Survival fraction – Point Sources.

The effect of the dose upon cell survival also needs to be compared to have an effective interpretation of the effects of these sources on tissue for brachytherapy planning considerations. One interesting example of dose not being equivalent to cell killing can be seen by comparing Figure 3-18 and Figure 3-19. ^{103}Pd imparts more dose to the surrounding tissue, but when it comes to cell survival fraction ^{125}I is actually better at destroying cells. While this sounds strange, it can easily be explained from the consideration of half-lives. ^{103}Pd has a half-life of 17 days whereas ^{125}I has a half-life of 59.4 days. The longer half-life of ^{125}I means that while

its initial dose rate may be lower than that of ^{103}Pd, ^{103}Pd will 'burn out' more quickly. Eventually ^{125}I will be imparting a greater dose rate than ^{103}Pd. In short ^{103}Pd does more damage initially, but ^{125}I does more damage in the long run.

Another major feature seen in Figure 3-19 is that as the killing range increases (radius of 10^{-9} cell survival fraction) the trend is that the slope of the survival curve between the killing range and the survival range (10^{-7} cell survival fraction) becomes much more gradual.

3.3.2. Two Source Studies

Just like in the simple shielding case, superposition was used to study the effect of two identical point sources moving toward each other for each isotope simulated.

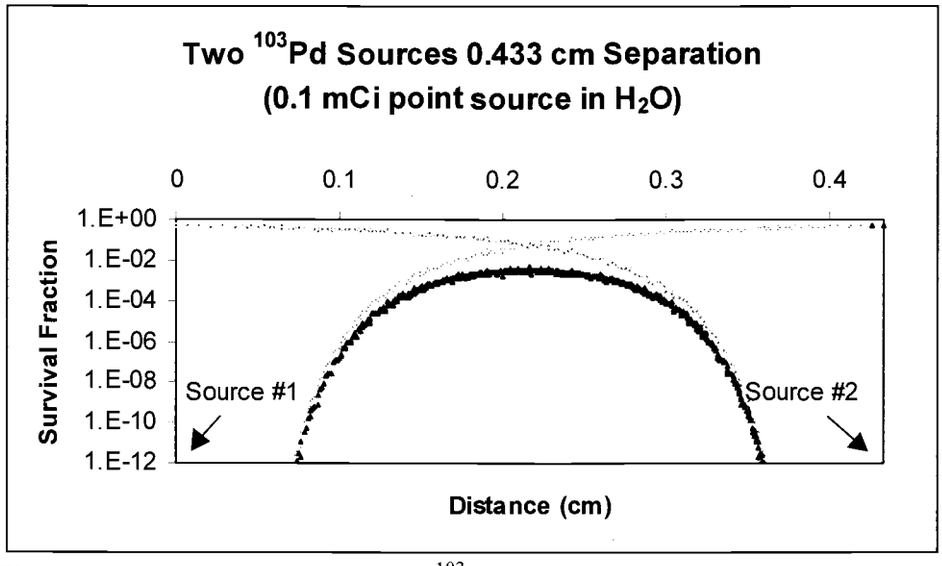

Figure 3-20. Two Source Studies – ^{103}Pd.

When two ^{103}Pd 0.1 mCi sources are placed 0.433 cm apart in an infinite medium of water the resultant distribution of cell survival fraction is that of Figure 3-20. It is interesting that at this separation the survival fraction peaks at about 10^{-2}, but the curve still mostly retains the shape of two independent point sources. The curve rises with the familiar shape then forms a plateau before decreasing again under the influence of the second source.

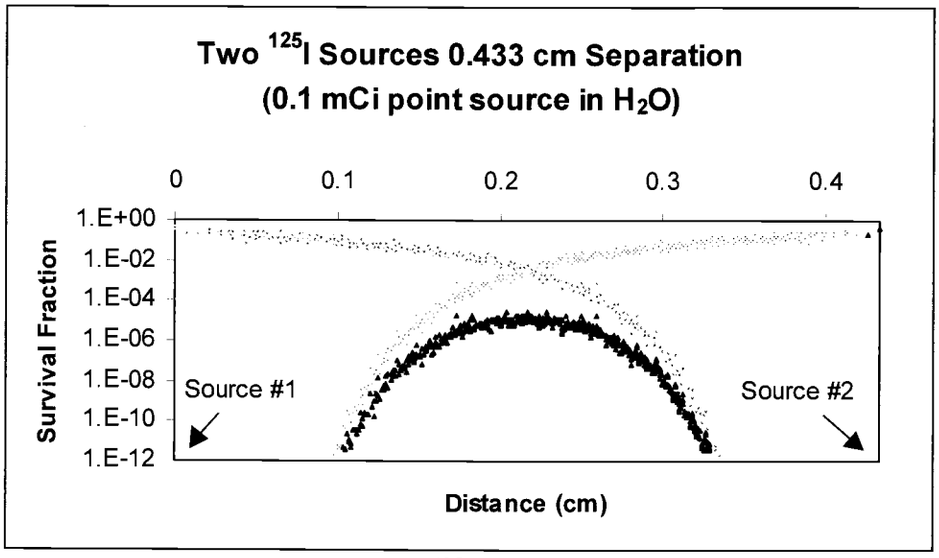

Figure 3-21. Two Source Studies – ^{125}I.

In Figure 3-21, the cell survival fraction peaks at about 10^{-5} cell survival fraction for two 0.1 mCi point sources of ^{125}I placed 0.433 cm apart. The ^{125}I survival fraction is about 3 orders of magnitude less than that of ^{103}Pd at the same source separation and the impact of greater damage region overlap can be seen on the shape of the curve in Figure 3-20. The survival curve of ^{125}I at a 0.433 cm source separation forms a much more arch-shaped curve than the ^{103}Pd does.

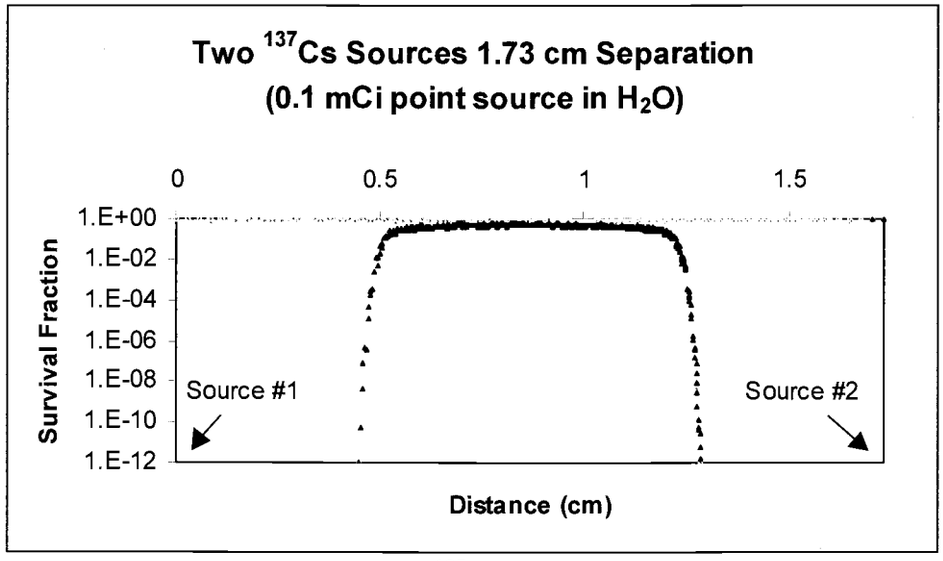

Figure 3-22. Two Source Studies – ^{137}Cs.

Figure 3-22 is a good illustration of the difference from the survival curves of gamma emitters. Two 0.1 mCi ^{137}Cs point sources at 1.73 cm spacing generate a survival curve peak at 57%. The curve has a plateau shaped peak instead of a more gentle arching curve consistent with a gamma emitter (for example ^{125}I in Figure 3-21). Another prominent feature of the two source ^{137}Cs survival curve is that the separation between sources is about 4 times greater than the separation between the two previously mentioned isotopes in this section. This is a good illustration of the effect of the larger range of ^{137}Cs.

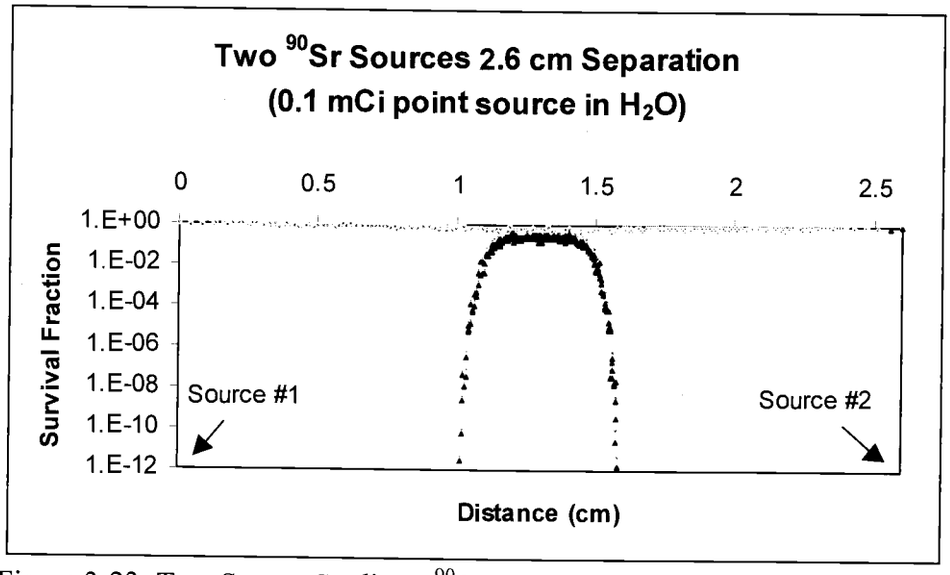

Figure 3-23. Two Source Studies – ^{90}Sr.

The last isotope to be considered here is a 0.1 mCi ^{90}Sr source. ^{90}Sr is also a beta emitter and also exhibits the much sharper curves in the damage region than would result from a gamma emitter. At the source separation of 2.6 cm shown in Figure 3-23, the two ^{90}Sr sources are too far away from each other to contribute a significant amount of dose to each other's damage region. This combined with the sharpness of the graph in the damage region creates an interesting plateau shape. This means that ^{90}Sr is a potentially 'precision' killing isotope.

3.4. Three Dimensional Source Arrays

Running individual point sources can take an immense amount of computer time (5000 minutes for a short run, 20000 minutes for a long run on a 750 Mhz

Spark), especially since electron interactions and secondary particles are sampled in detail, especially for analog Monte Carlo (no variance reduction). Because of this a single source was calculated, and its results were then post processed with an external program to superimpose the dose fields from multiple sources and recalculate the survival curves. This section studies the effect that deviations of seed placement (one seed displaced) have upon dose and survival curves in a three dimensional matrix.

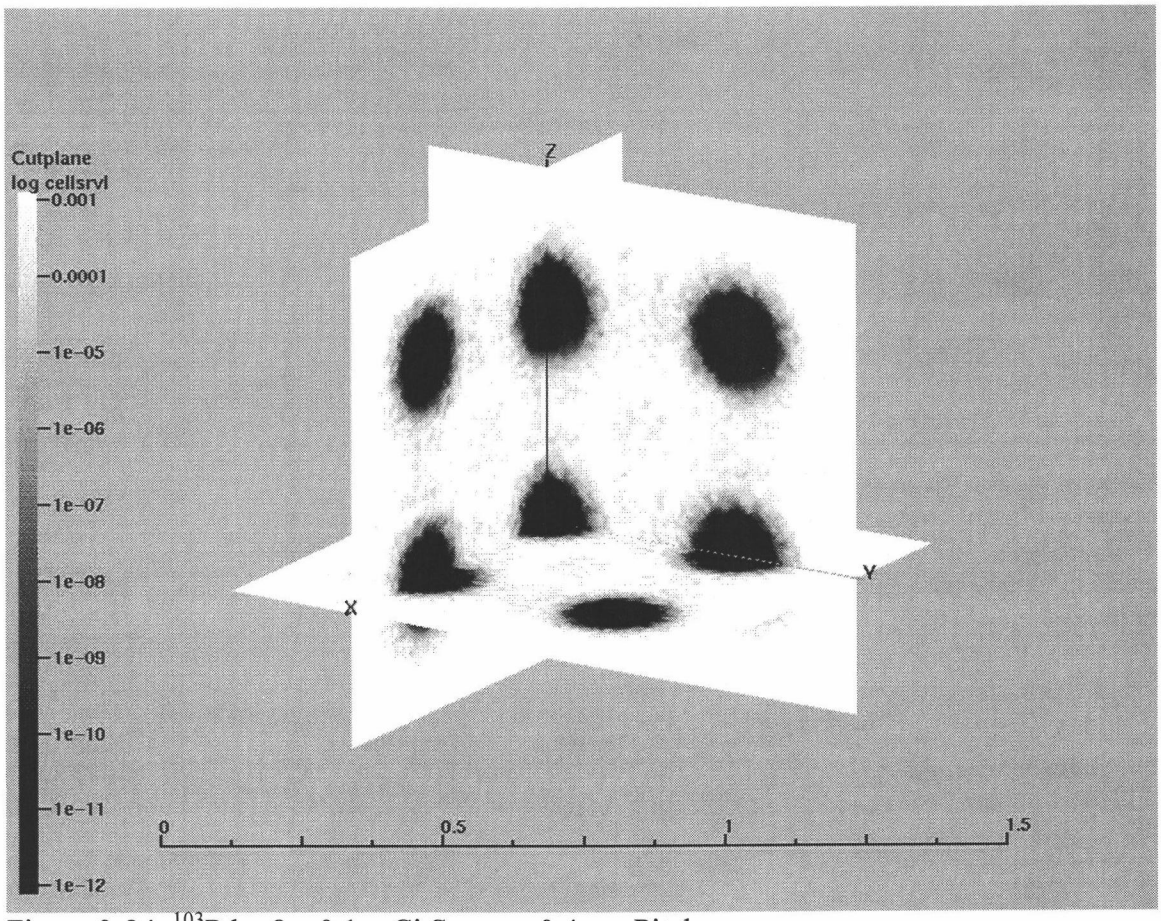

Figure 3-24. ^{103}Pd – 8 – 0.1 mCi Sources 0.4 cm Pitch.

Figure 3-24 is a three dimensional visualization of cell survival probabilities for ^{103}Pd. At a pitch (center-to-center spacing) of 0.4 cm it shows little overlap between neighboring sources. At distances greater than 0.3 cm the 0.1 mCi sources do not have a significant effect on cell survival.

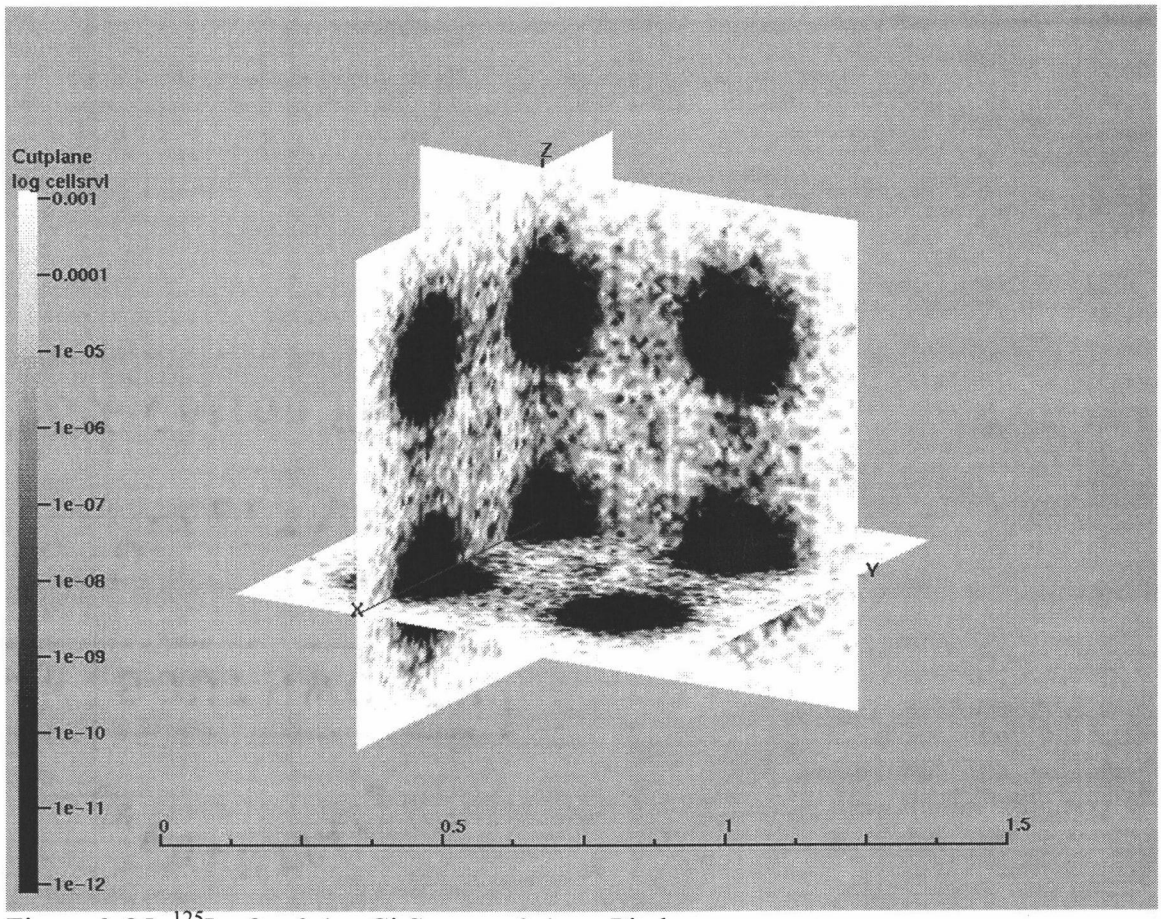

Figure 3-25. ^{125}I – 8 – 0.1 mCi Sources 0.4 cm Pitch.

The pitch used for the ^{125}I sources is the same as that for ^{103}Pd, 0.4 cm. Both isotopes have similar dose and cell survival curves. ^{103}Pd has a slightly greater initial

dose rate, but ^{125}I has a greater effect on cell killing. This can be seen in Figure 3-25. The same scales were used in both figures.

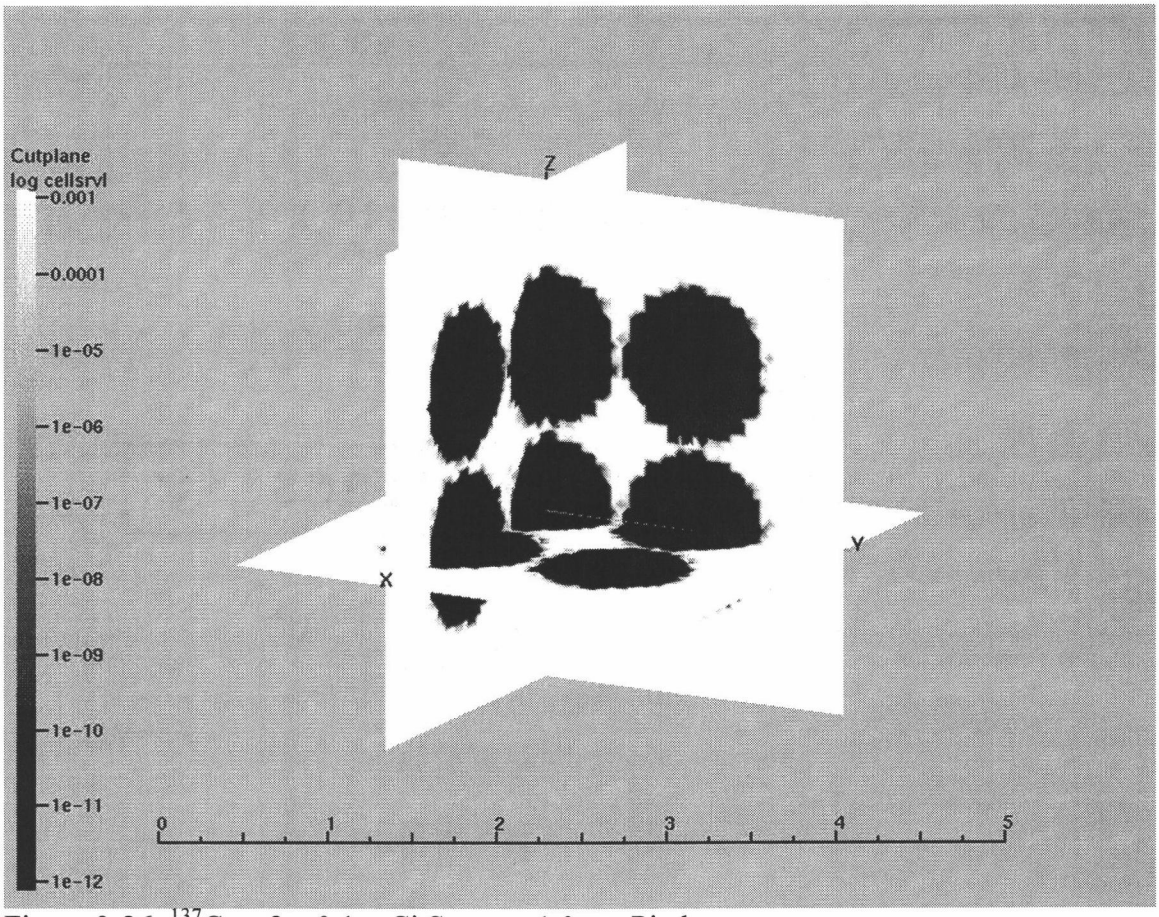

Figure 3-26. ^{137}Cs – 8 – 0.1 mCi Sources 1.0 cm Pitch.

Figure 3-26 shows an array of 8 ^{137}Cs sources with a pitch of 1.0 cm. When Figure 3-26 is compared to 3-24 and 3-25 it can be seen that the range of ^{137}Cs is much greater than that of ^{103}Pd or ^{125}I. Also of interest is the fact that the edges of the cell killing range are much sharper for ^{137}Cs (electron emitter) than for the photon emitting isotopes shown (^{103}Pd and ^{125}I). This can be attributed to the 'drag' on

electrons caused by Coulomb forces causing them to stop in shorter distances than uncharged particles such as photons.

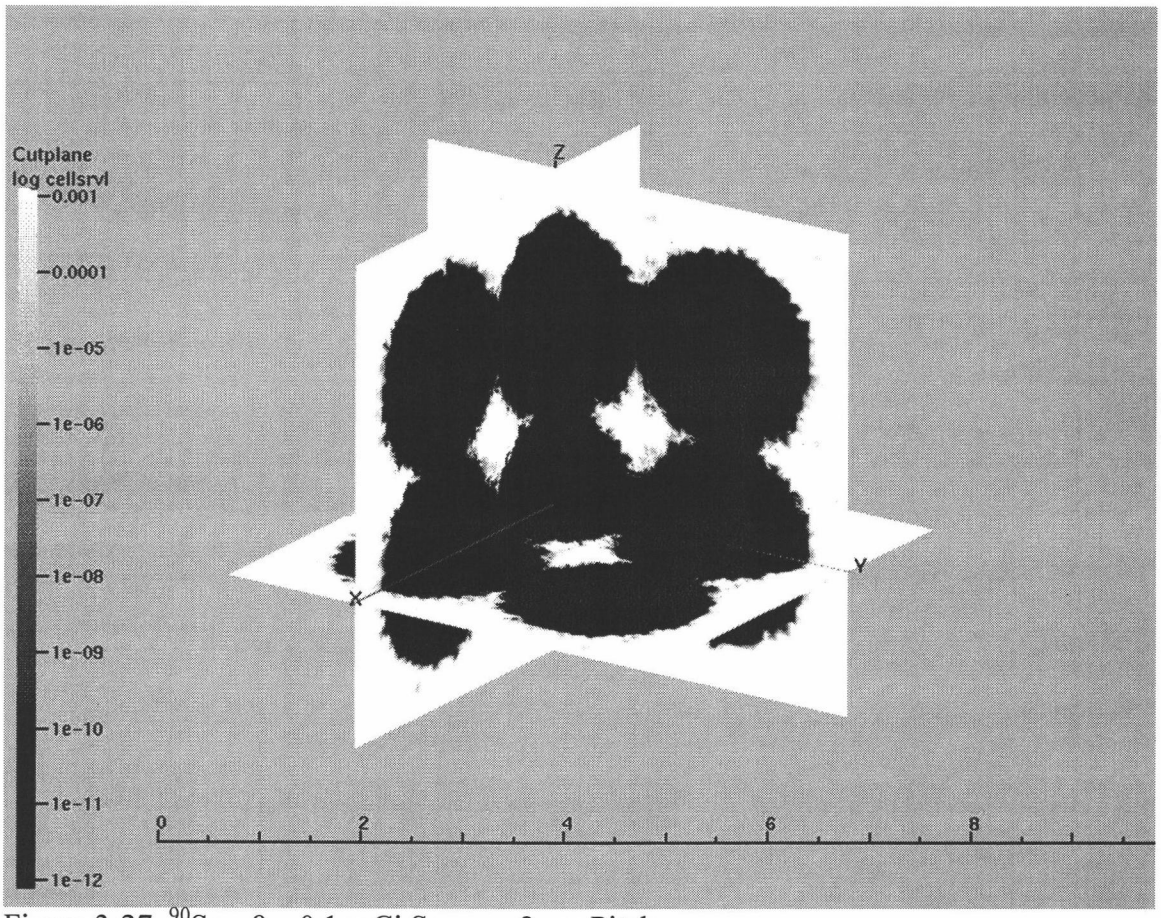

Figure 3-27. ^{90}Sr – 8 – 0.1 mCi Sources 2 cm Pitch.

The last isotope to be considered in this section is ^{90}Sr. Figure 3-27 shows the ^{90}Sr sources placed with a 2 cm pitch, much larger than any of the other sources studied in this thesis. This extra range is attributed to the decay of the daughter of ^{90}Sr, ^{90}Y. ^{90}Y has a maximum electron emission energy of 2.28 MeV (Martin 2000), which is huge compared to that of ^{137}Cs (maximum electron energy of 1.18 MeV (Martin 2000. ^{90}Sr also shows the sharp edges on the killing range.

3.5. Superposition

Superposition of the dose was used as an assumption for the previous multiple source problems. The reason that it was used is because the simulation time for one point source was immense (5000 to 20000 minutes). The simulations were run with the PENELOPE code and then post processed with a secondary code to superimpose dose rates from different sources upon each other. Then the cell survival fraction was recalculated. To test the validity of the superposition assumption, a calculation was performed (see Table 3-5) with two ^{3}H point sources. The result from single source calculations was compared to the two source calculation.

Isotope	Particle Type	Initial Activity (Ci)	k (hr^{-1})	λ (hr-1)	α (Gy^{-1})	β (Gy^{-2})
^{3}H	e^{-}	10^{-16}	6.42E-6	1.5	0.1	0.01

Table 3-5. Values Used for Superposition Test Problem.

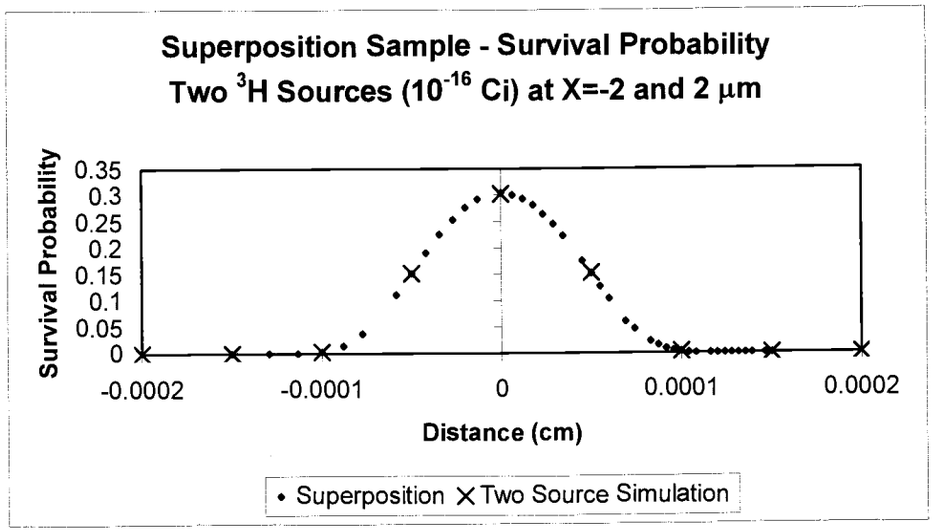

Figure 3-28. Superposition Sample Problem.

Figure 3-28 shows the data generated by a simulation of two point sources of 3H (the X's) with coordinates of -0.0002,0,0 cm and 0.0002,0,0 cm, and the data from a single point source (the dots) reprocessed and superimposed upon the other source with a spread of 0.0004 cm. As can be seen from Figure 3-28, there are no significant differences between the two different methods. Therefore superposition is a reasonable assumption.

3.6. Summary

This chapter describes the results of a simple point source model used to predict the approximate shape of the dose and cell survival curves that the simulated sources would show. The effect of a second source influencing the cell survival curve

was considered. Parametric studies were performed to examine the effects of changes of various parameters that influence the shape of the cell survival curve. Several point sources (^{103}Pd, ^{137}Cs, ^{90}Sr, and ^{125}I) were run using the PENELOPE code to model the dose and cell survival curves. Superposition was used to simulate a second identical point source near the first one and the impact of the proximity of the second source on the cell survival curves was shown. Superposition was again used to superimpose multiple point sources in three-dimensional space and 3D maps of cell survival fraction are shown for each isotope. This chapter ends with a sample problem using a ^{3}H source to double check if superposition is a reasonable assumption to use for the problems presented in this thesis.

4. Conclusions and Recommendations for Future Work

4.1. Conclusions

The questions proposed in this thesis are:

- What resolution is needed (how small does a voxel need to be) to allow the change in dose between neighboring voxels to be small (less than 10%),
- What is the killing range of the different isotopes studied,
- How do the shapes of the dose and cell survival fraction curves compare, and
- How do small deviations in placement of sources affect the cell survival fraction curve?

Resolution studies were started, but were discontinued for the following reasons: experimentation with the PENELOPE code showed that as the voxel size was decreased, the dose to the voxel in which the source was positioned would increase without bound (see Equation 2-1). This in an artifact of a size reduction of the voxel in which the point source is located in, and is not physical. The brachytherapy seeds have a finite volume that tissue does not occupy; therefore, the question that should have been asked is "What resolution is required such that, in the tissue being irradiated, dose changes between neighboring voxels is kept small?" Another issue concerning voxel size is that as the length of a side of a voxel is halved,

the volume of the voxel decreases by an eighth. If the volume decreases by a factor of eight, eight times the number of voxels are required to map the same region. Eight times the number of simulated tracks also need to be run to achieve approximately the same statistics. This means that if the length of a side of a voxel is halved, the simulation will need to run eight times as long.

The sources studied in this thesis were all simulated with the same initial activity (0.1 mCi). Their relative kill (survival fraction of 10^{-9}) and survival (survival fraction of 10^{-7}) ranges are summarized in Table 4-1. It was found that the gamma emitting sources (^{103}Pd and ^{125}I) had much shorter ranges than the beta emitting sources (^{137}Cs and ^{90}Sr). This can be attributed more to emission energy and half-life than to particle type. Although, when the damage region is divided by survival radius it is found that the beta emitting isotopes have a much smaller damage region relative to their survival radius. It would be interesting to see more isotopes of each type compared and to assess the variation across a larger sample of isotopes.

Isotope	Kill Radius (cm)	Survival Radius (cm)	Damage Region Thickness (cm)	Damage Region / Survival Radius
^{103}Pd	0.087	0.094	0.007	0.074
^{125}I	0.115	0.129	0.014	0.109
^{137}Cs	0.456	0.461	0.005	0.011
^{90}Sr	1.023	1.034	0.011	0.011

Table 4-1. Kill and Survival Radius.

The shapes of the dose and cell survival fraction curves have been shown in detail in Chapter 3 (Results). The dose curve drops off as an exponential decay with increasing distance from the source. The cell survival fraction curve starts at zero chance of survival near the source. Upon reaching a distance sufficiently far away from the source, the cell survival fraction curve begins to increase rapidly reaching a value of 100% cell survival.

Through studies involving two sources in close proximity to each other it was found that small deviations in placement can have very large effects on cell killing. This occurs because the survival curves are extremely steep. When sources have a spacing larger than the 95% survival radius, they behave as if they are independent. When their spacing is less than that of the kill radius then everything is destroyed between the two sources, but everything in that region would be destroyed by a single source. Again this scenario is uninteresting. The interesting situation occurs when the two sources approximately have their individual 10^{-5} survival radii overlapping. In this case cells within the damage region of both sources are more effectively killed than if it were merely within the range of just one source.

Many trends important to an understanding of brachytherapy were investigated during the course of this work. The simple shielding problem was effective in studying trends achieved by manipulating certain variables:

- As intensity is increased, the kill radius increases,
- As the shielding attenuation factor is increased, the kill radius decreases,
- As the linear lesion coefficient increases, the kill radius increases,
- As the quadratic lesion coefficient increases, the kill radius increases slightly, and the damage region thickness decreases slightly,
- As the isotopic decay constant increases ($t_{1/2}$ decreases) , the kill radius decreases, and
- As the rate of DNA damage repair increases (tissue repair half-time decreases), the kill radius decreases slightly.

The PENELOPE brachytherapy calculations also presented some lessons that are important to take into account when planning a brachytherapy treatment. The decay constant of the radioisotope source has a pronounced effect on the cell survival radius (see Figures 3-12 and 3-13). Figure 3-12 shows that ^{103}Pd deposits more dose in the surrounding tissue initially, but because of its large decay constant (small $t_{1/2}$) it decays rapidly and 'burns out'. As a result, it actually has less of an effect on cell killing than ^{125}I (see in Figure 3-13).

The type of particle emitted also significantly effects the shape of cell survival curves. Beta emitting radioisotopes have curves with a sharper distinction between the kill radius and the survival radius. This effect can be explained by the fact that photons must undergo collisions to deposit their energy, whereas electrons

continuously interact with the surrounding materials through Coulomb interactions. These Coulomb interactions act as a drag bringing low energy electrons to a stop in a shorter distance than for similar low energy photons and depositing the energy in a more confined region in the material.

4.2. Recommendations for Future Work

There are several issues that need to be addressed to take the next few steps in this work. Improvements in the PENELOPE code that could be implemented for better results are: use of a more complicated cell survival model, and support for modeling of different material regions and geometries.

One of the shortcomings of this research is that the ^{137}Cs source definition excluded several x-rays. The impact of these x-rays on the cell survival curve is unknown, and should be investigated. Studies should also be performed to compare the accuracy of the output data for various choices of the energy cutoffs. Increasing the cutoffs decreases computational time at the cost of accuracy. If a good 'rule of thumb' can be developed, simulation times can be decreased while maintaining confidence in the accuracy of the results.

The post processing code that needs the most work is the code that performs the 3D mapping of the individual sources. Data from the single source simulation is

mapped to the locations where all the sources in the specified array lie, then it adds the doses in the overlapping regions. With a large number of sources, this process is very slow when plotting in 3D because of the immense number of overlapping vertices/cells. If the duplicated points were eliminated at the end of the post processing code, 3D visualization could be accelerated.

The primary improvement needed in the PENELOPE code is implementation of material regions and geometries. Adding support for different material regions and geometries would allow a much more faithful representation of the brachytherapy seeds, and the surrounding tissue. Another potentially useful addition to the PENELOPE code would be to use a more accurate/complicated cell survival correlation, preferably one that includes repopulation. If repopulation is included, the effect of decay constants on cell survival distributions may be significantly different than that calculated in this study.

Biblography

(ACS 2003) American Cancer Society. "Cancer Facts and Figures 2003". (2003).

(Armpilia 2003) Armpilia, C. I. "The Determination of Radiobiologically Optimized Half-Lives for Radionuclides Used in Permanent Brachytherapy Implants". Int. J. Radiation Oncology Biol. Phys. v. 55. n. 2. p. 378-385. (2003).

(Arnfield 2002) Arnfield, M. R. et al. "The Effect of High-Dose-Rate Brachytherapy Dwell Sequence on Cell Survival". Int. J. Radiation Oncology Biol. Phys. v. 52. n. 3. p. 850-857. (2002).

(Asenjo 2002) Asenjo, J., Fernandez-Varea, J. M., Sanchez-Reyes, A. "Characterization of a High-Dose-Rate ^{90}Sr-^{90}Y Source for Intravascular Brachytherapy by Using the Monte Carlo Code PENELOPE". Pysics in Medicine and Biology. v. 47. p. 697-711. (2002).

(Brenner 1995) Brenner D. J., Hlatky L. R., Hahnfeldt P. J., Hall E. J., Sachs R. K. "A Convenient Extension of the Linear-Quadratic Model to Include Redistribution and Reoxygenation". Int. J. Radiation Oncology Biol. Phys. v. 32. n. 2. p. 379-90. (May 15, 1995).

(Briesmeister 2000) Briesmeister J. F., Ed., "MCNP - A General Monte Carlo N-Particle Transport Code". Los Alamos National Laboratory Report, LA-13709-M (April, 2000).

(Chen 1996) Chen, J., Nekolla, E., Kellerer, A. M. "A Comparative Study of Microdosimetric Properties of x-rays, γ-rays, and β-rays". Radiat. Environ. Biophys. v. 35. p. 263-266. (1996).

(Mainegra 1998) Mainegra, E., Capote, R., Lopez, E. "Dose Rate Constants for ^{125}I, ^{103}Pd, ^{192}Ir, and ^{169}Yb Brachytherapy Sources: an EGS4 Monte Carlo Study". Phys. Med. Biol. v. 43. p. 1557-1566. (1998).

(Martin 2000) Martin, J. E. "Physics for Radiation Protection". John Wiley & Sons, Inc. New York. (2000).

(Nahum 1996) Nahum, A. E. "Microdosimetry and Radiocurability: Modeling Targeted Therapy with β-emitters". Phys. Med. Biol. v. 41. p. 1957-1972. (1996).

(Nath 1995) Nath R., Anderson, L. L., Luxton, G., Weaver, K. A., Williamson, J. F., Meigooni, A. S. "Dosimetry of Interstitial Brachytherapy Sources". AAPM Report n. 51. (March 1995).

(Parrington 1996) Parrington, J. R., Knox, H. D., Breneman, S. L., Baum, E. M., Feiner, F. "Nuclides and Isotopes". Fifteenth Edition. Lockheed Martin. (1996).

(Rivard 2003) Rivard, M. J., Kirk, B. L., Leal L. C. "Dependence of Brachytherapy Dosimetry on the Uniformity of the Isotope Physical Distribution". Nuclear Mathematical and Computational Sciences: A Century in Review, A Century Anew. (April 6-11, 2003).

(Sachs 1997) Sachs R. K., Hahnfeld P., Brenner D. J. "The Link Between Low-LET Dose-Response Relations and the Underlying Kinetics of Damage Production/Repair/Misrepair". Int J Radiat Biol. v. 72. n. 4. p. 351-74. (Oct 1997).

(Salvat 2001) Salvat, F., Fernandez-Varea, J. M., Acosta, E., Sempau, J. "PENELOPE – A Code System for Monte Carlo Simulation of Electron and Photon Transport". Nuclear Energy Agency. (November 2001).

(Veninga 2001) Veninga, T., Visser, A.G., Van den Berg A. P., Van Hooije, C. M. C., Van Geel, C. A. J., Levendag, P. C. "Equivalence of Hyperfractionated and Continuous Brachytherapy in a Rat Tumor Model and Remarkable Effectiveness when Preceded by External Irradiation". International Journal of Radiation Oncology Biology Physics. v. 49. n. 5. p. 1351-1360. (Apr 1, 2001).

(Wang 2003) Wang J. Z., Guerrero M., Li X. A. "How Low is the α/β Ratio for Prostate Cancer?" Int J. Radiation Oncology Biol. Phys. v. 55. n. 1. p. 194-203. (Jan 1, 2003).

(Wu 2002) Wu Q, Mohan R, Niemierko A, Schmidt-Ullrich R. "Optimization of Intensity-Modulated Radiotherapy Plans Based on the Equivalent Uniform Dose". Int. J Radiation Oncology Biol. Phys. v. 52. n. 1. p. 224-235. (Jan 1, 2002).

Appendices

A. Derivation of Dose Protraction Factor for Radiation Pulse

The equation for the dose protraction factor is as follows:

$$G = \frac{2}{D^2} \int_{-\infty}^{\infty} \dot{D}(t) \int_{-\infty}^{t} e^{-\lambda(t-t')} \dot{D}(t') dt' dt \,, \tag{A-1}$$

where D is the total dose (Gy), $\dot{D}(t)$ is the dose rate (Gy/hr) at time t (hr), and λ is the DNA repair constant (hr^{-1}).. The dose rate for a radiation pulse from $t=0$ to $t=t_f$ is defined as follows:

$$\dot{D}(t) = D_0 \,, \tag{A-2}$$

where D_0 (Gy/hr) is a constant, and the total dose $D=D_0 * t_f$. Inserting Equation A-2 into A-1 and changing the limits of the integrals to values at which the pulse function is non-zero,

$$G = \frac{2}{(D_0 t_f)^2} \int_{0}^{t_f} D_0 \int_{0}^{t} e^{-\lambda(t-t')} D_0 dt' dt \,. \tag{A-3}$$

Simplifying Equation A-3,

$$G = \frac{2}{t_f^2} \int_0^{t_f} e^{-\lambda t} \int_0^{t} e^{\lambda t'} dt' dt . \tag{A-4}$$

Integrating and applying the limits of the inner integral,

$$G = \frac{2}{t_f^2} \int_0^{t_f} e^{-\lambda t} \frac{\left(e^{\lambda t} - 1\right)}{\lambda} dt . \tag{A-5}$$

Simplifying Equation A-5,

$$G = \frac{2}{\lambda t_f^2} \int_0^{t_f} \left(1 - e^{-\lambda t}\right) dt . \tag{A-6}$$

Integrating the second integral and applying the limits,

$$G = \frac{2}{\lambda t_f^2} \left(t_f + \frac{e^{-\lambda t_f}}{\lambda} - \frac{1}{\lambda} \right). \tag{A-7}$$

The final result for the dose protraction factor for a pulse of duration t_f is,

$$G = \frac{2}{\left(\lambda t_f\right)^2} \left(t_f \lambda + e^{-\lambda t_f} - 1 \right), \tag{A-8}$$

B. Derivation of Dose Protraction Factor for Exponential Decay

The equation for the dose protraction factor is as follows:

$$G = \frac{2}{D^2} \int_{-\infty}^{\infty} \dot{D}(t) \int_{-\infty}^{t} e^{-\lambda(t-t')} \dot{D}(t') dt' dt \,, \tag{B-1}$$

where D is the total dose (Gy), $\dot{D}(t)$ is the dose rate (Gy/hr) at time t (hr), and λ is the DNA repair constant (hr^{-1}). The dose rate for an exponential decay beginning at $t=0$ is defined as follows:

$$\dot{D}(t) = D_0 e^{-kt} \,, \tag{B-2}$$

where D_0 is the initial dose rate (Gy/hr) and k is the isotope decay constant (hr^{-1}). Substituting Equation B-2 into B-1 and changing the integral limits for the time at which the source is non-zero ($t \geq 0$) then,

$$G = \frac{2}{(D_0 / k)^2} \int_{0}^{\infty} D_0 e^{-kt} \int_{0}^{t} e^{-\lambda(t-t')} D_0 e^{-kt'} dt' dt \,. \tag{B-3}$$

Simplifying,

$$G = 2k^2 \int_0^{\infty} e^{-(k+\lambda)t} \int_0^{t} e^{(\lambda-k)t'} dt' dt . \qquad \text{(B-4)}$$

Solving the inner integral and applying the limits,

$$G = 2k^2 \int_0^{\infty} e^{-(k+\lambda)t} \frac{1}{\lambda - k} (e^{(\lambda-k)t} - 1) dt . \qquad \text{(B-5)}$$

Simplifying,

$$G = \frac{2k^2}{\lambda - k} \int_0^{\infty} (e^{-2kt} - e^{-(k+\lambda)t}) dt . \qquad \text{(B-6)}$$

Solving the remaining integral and applying the limits,

$$G = \frac{2k^2}{\lambda - k} \left(\frac{1}{2k} - \frac{1}{\lambda + k} \right). \qquad \text{(B-7)}$$

The final result for the dose protraction factor for an exponentially decaying source beginning at $t=0$ and allowed to decay to infinity is,

$$G = \frac{k}{\lambda + k} . \qquad \text{(B-8)}$$